Chapter 3

SILICATE PRECIPITATION MEDIATED BY ANME-SRB CONSORTIA

Kyle S. Metcalfe[1], Daniela Osorio Rodríguez[1], Hank Yu[1], Anne E. Dekas[2], Shawn E. McGlynn[3], John P. Grotzinger[1], and Victoria J. Orphan[1]

[1] Division of Geological and Planetary Sciences,
California Institute of Technology, Pasadena, California, 91125

[2] Department of Earth System Science,
Stanford University, Stanford, California, 94305

[3] Earth-Life Science Institute,
Tokyo Institute of Technology, Ookayama, Meguro, Tokyo, 152-8550, Japan

ABSTRACT

Prokaryotic silicate biomineralization in solutions undersaturated with respect to amorphous silica—representative of conditions in most shallow sediment pore waters—is poorly understood, but may be significant for the preservation of microfossils and soft tissues in the rock record by early silicate cementation. Recent work reported the presence of authigenic silicates (clays) attached to the exteriors of consortia of anaerobic methane-oxidizing archaea (ANME) and sulfate-reducing bacteria (SRB). However, it remains uncertain whether the association between ANME-SRB consortia and silicates occurs through biogenetic precipitation or represent passive attachment if detrital sedimentary particles. In this study, we addressed the null hypothesis of abiotic silicate attachment and/or precipitation to consortium surfaces by characterizing the texture and composition of ANME-SRB consortium-attached silicates sourced directly from deep-sea methane seep

sediments and from 3-year-long sediment-free enrichments of methane-oxidizing ANME-SRB consortia in Si-poor artificial seawater. Compositional data from both field-collected and sediment-free consortia demonstrates statistically significant ($p < 0.01$) Si enrichment in consortium-attached silicates over detrital silicates drawn from the same sample. The texture of silicate phases attached to ANME-SRB consortia maintained anaerobically in sediment-free conditions is distinct from that observed *in situ* and suggests the growth of these phases concomitant with AOM consortia growth over a 3 year period at 10˚ C. ICP-MS measurements of media [Si] in sediment-free incubations preclude Si enrichment via abiotic silica precipitation or Si adsorption to clays. Instead, these laboratory controlled incubations suggest AOM consortia mediate silicate biomineralization in conditions undersaturated with respect to precipitation of amorphous silica as well as equilibrium silicon adsorption onto clays, and thus may point to a previously underexamined mode of biomineralization by microorganisms abundant in methane-rich marine sediments.

INTRODUCTION

The anaerobic oxidation of methane (AOM) is an important, microbially-driven process modulating methane flux from coastal sediments worldwide. AOM consumes 80-90% of CH_4 produced in marine sediments (Reeburgh, 2007; Knittel and Boetius, 2009), oxidizing methane to bicarbonate via the reduction of sulfate to sulfide:

$$CH_4 + SO_4^{2-} \rightarrow HCO_3^- + HS^- + H_2O \qquad \Delta G = -10 \text{ to } -40 \text{ kJ mol}^{-1}.$$

The scant energy produced by this reaction, barely sufficient for ATP synthesis (Schink, 1997), is harnessed by multicellular methane-oxidizing archaea (ANME) and sulfate-reducing bacteria (SRB) consortia common in methane seep ecosystems, reaching maximum abundances on the order of 10^7 consortia per cm^3 of sediment (Boetius et al., 2000; Orphan et al., 2001b, 2002). ANME-SRB cell aggregation likely enables direct interspecies electron transfer between ANME and SRB (McGlynn et al., 2015; Wegener et al., 2015). Experimental evidence demonstrating the capacity for ANME-SRB consortia to reduce solid phase iron and manganese oxides (Beal et al., 2009; Cai et al., 2018; Leu et al., 2020) supports this model and further suggests interactions between ANME-SRB consortia and mineral electron acceptors in the environment.

Traditionally, studies of the interactions between ANME-SRB consortia and minerals have focused on the precipitation of authigenic carbonates resulting from alkalinity production via AOM. The production of bicarbonate and sulfide ion increases porewater alkalinity in zones of AOM activity, driving the precipitation of carbonate minerals (Luff and Wallmann, 2003). Extensive seafloor pavements observed proximal to

sites of CH_4 seepage are thought to be the result of pervasive cementation of terrigenous clastic sediment by AOM-induced carbonate precipitation (Aloisi et al., 2000; Luff and Wallmann, 2003; Teichert et al., 2005; Naehr et al., 2007). Geochemical modeling of seep carbonate porewaters (Luff and Wallmann, 2003) and nonequilibrium clumped isotope signatures in modern and ancient seep carbonates imply rapid carbonate precipitation rates during early diagenesis (Loyd et al., 2016; Thiagarajan et al., 2020), suggesting interactions between ANME-SRB consortia and authigenic mineral precipitation at seeps. Indeed, many studies demonstrate the presence of viable ANME consortia and active AOM in association with seep carbonates and carbonate concretions (Marlow et al., 2014; Case et al., 2015; Mason et al., 2015), in some cases forming large 'reefs' in which a carbonate pillar protruding from the seafloor is coated in ANME microbial mats (Michaelis et al., 2002; Treude et al., 2007). Given these observations, one might expect carbonate minerals to associate with EPS coatings on ANME-SRB consortia, as SRB cell surface and/or EPS chemistry has been suggested to catalyze carbonate precipitation (Visscher et al., 2000; Braissant et al., 2007; Decho, 2010; Krause et al., 2012).

It is therefore surprising that silicate phases are more commonly found intimately associated with ANME-SRB consortia than carbonate phases (Pernthaler et al., 2008; Dekas, 2013; Chen et al., 2014). These observations were initially collected by correlated fluorescence in situ- hybridization (FISH), scanning electron microscopy (SEM), and nanoscale secondary ion mass spectroscopy (nanoSIMS) analysis (for Si), which revealed the common presence of a Si-rich phase surrounding consortia sourced directly from sediments. Initial energy-dispersive spectroscopy (EDS) analysis characterized this silicate

phase as an aluminosilicate clay (Dekas, 2013). Further SEM-EDS analysis revealed the presence of a texturally-massive Si-rich phase between Al-rich phases within the silicate shell, interpreted as a silica cement binding detrital aluminosilicate clays to ANME-SRB consortium exteriors (Chen et al., 2014). Alkalinity produced by AOM was proposed to drive diatom frustule dissolution via increased pH of porewater, followed by Si precipitation on ANME-SRB consortium exteriors due to interactions with adsorbed metal cations such as Al (Chen et al., 2014).

The hypothesis that silica precipitation on ANME-SRB consortia is enhanced by alkalinity-driven silica leaching is notable in that it implies prokaryotic silica biomineralization occurring in porewater undersaturated with respect to amorphous silica, an understudied process about which little is known. Previous research on prokaryotic silica and silicate biomineralization has focused predominantly on phases precipitated from solutions supersaturated with respect to amorphous silica (Phoenix et al., 2002, 2003; Yee et al., 2003; Lalonde et al., 2005; Hugo et al., 2011) or on cell-associated clay or clay-like phases rich in Fe and Al (Ferris et al., 1987; Konhauser et al., 1993, 1994; Mera and Beveridge, 1993; Köhler et al., 1994, 1999; Urrutia and Beveridge, 1994; Konhauser and Urrutia, 1999; Fein et al., 2002). Experimental work examining precipitation from supersaturated Si solutions demonstrated most precipitation to occur in solution abiotically, independent of the presence of bacterial cells (Yee et al., 2003) (Phoenix et al., 2003; Yee et al., 2003). In experiments examining silicate precipitation in solutions undersaturated with respect to amorphous silica, the coating of *Bacillus subtilis* cell surfaces by synthetic iron oxides was required to adsorb significant Si to cells (Fein et al., 2002), producing

silicate precipitates rich in Fe and/or Al on cell surfaces, similar to some phases observed attached to cells sampled from sediments (Konhauser et al., 1993, 1994; Köhler et al., 1994; Konhauser and Urrutia, 1999). However, in these experiments, control incubations in which the iron oxide coating was added alone removed significant Si from solution, indicating the interaction between Fe and Si occuring at the cell surface is unlikely to have any biotic influence. These experimental results are consistent with previous work demonstrating that in the presence of Al or Fe oxides or clay minerals, Si solubility is considerably reduced from Si solubility with respect to amorphous silica (Siever and Woodford, 1973; Iler, 1979).

Surprisingly, silicate phases observed on ANME-SRB consortium exteriors are Fe- and Al-poor (Dekas, 2013; Chen et al., 2014), and sediment porewaters are often below theoretical silica saturation (~1170 μM at pH 8, 4˚ C (Gunnarsson and Arnórsson, 2000)) due to interactions with Al from detrital clays (Van Cappellen and Qiu, 1997; Dixit et al., 2001; Michalopoulos and Aller, 2004; Tréguer and De La Rocha, 2013). For context, methane seep sediment porewater [Si] has been measured at ~400 μM (Zabel et al., 2008). Any model explaining precipitation of Si-rich silicate phases on ANME-SRB consortium exteriors must therefore depart from current understandings of prokaryotic silicate biomineralization developed through examination of cell-associated Fe- and/or Al-rich clay-like phases or silicate precipitation occurring under conditions supersaturated with respect to amorphous silica.

To date, observations of silicate phases adhered to ANME-SRB consortia have been acquired from samples isolated directly from clay-rich seep sediments (Dekas et al.,

2009; Zhang et al., 2010, 2011; Dekas, 2013; Chen et al., 2014), preventing clear discrimination of active, biologically-mediated precipitation from passive attachment of phases to cell exteriors. The latter process is a null hypothesis at once important and challenging to reject, as passive abiotic attachment can result in intimate spatial association between minerals and cell exteriors (Glasauer et al., 2001), confounding textural analysis in the absence of additional geochemical or microbiological constraints on porewater composition or cell growth.

Here we attempted to investigate the proposed hypotheses (Dekas, 2013; Chen et al., 2014) of ANME-SRB consortium-mediated silicate precipitation through direct microscopy and analysis of the exteriors of active ANME-SRB consortia separated from methane seep sediments and maintained in laboratory incubations in media with [Si] below the threshold for abiotic silica precipitation or Si adsorption to preexisting, consortium-attached aluminosilicates. We found the growth of abundant Si-rich phases embedded in EPS and attached to ANME-SRB consortium exteriors with compositions (1) significantly Si-enriched relative to the Si content of the original source sediment and (2) similar to those of silicate phases found adhered to ANME-SRB consortia sourced directly from diverse seep sediment. These observations demonstrated de novo growth of a Si-rich silicate phase from solutions undersaturated with respect to amorphous silica, and suggestive of bona fide silicate biomineralization mediated by ANME-SRB consortia both in culture experiments and in a diversity of methane seep sediments.

MATERIALS AND METHODS

Sample Collection and Processing

Sediment samples analyzed in this study were collected by push coring using the submersible HOV *Alvin* of the R/V *Atlantis* from 2 seafloor methane seep sites, in the Eel River Basin (AT 15-11, October 2006) and off the coast of Costa Rica (AT 37-13, May 2017), and by the ROV *Doc Ricketts* of the R/V *Western Flyer* from a seafloor methane seep site in Santa Monica Basin (October 2013). Push core (PC) samples PC14 and PC15 from *Alvin* dive AD4254 (AT 15-11) were collected from a microbial mat proximal to an active methane seep site 520 m below sea level (mbsl) on the Northern Ridge of Eel River Basin (40.786533, -124.5951). Samples from the Costa Rica Margin (AT 37-13) were obtained during *Alvin* dive AD4912 from a microbial mat (PC 6) collected at 1811 mbsl in the Jacó Scar submarine landslide (9.1163, -84.8372). Samples from Santa Monica Basin were covered in a microbial mat at a seafloor methane seep site (33.788835, -118.668298) at 863 mbsl during DR 459 (PC 43). In all cases, samples were processed shipboard by extruding sediment upward from the push core liner and sectioning sediment at 3 cm intervals. Subsamples of sediment were frozen at -80˚ C, PFA-fixed for microscopy, or sealed in Ar-sparged mylar bags and stored at 4˚ C for laboratory-based microcosm experiments.

Carbonate rock samples analyzed in this study were collected using the robotic arm of HOV *Alvin* from a seafloor methane seep site in the Jacó Scar off the coast of Costa Rica during the R/V *Atlantis* cruise AT42-03. Sample #10860 was collected from a warm (6˚ C) seep site at 1784 mbsl (9.117783, -84.839512), and processed shipboard by placing in a

mylar bag filled with Ar-sparged, filter-sterile seawater collected by Niskin bottle. The mylar bag was supplied with CH_4 and stored at 4˚ C for laboratory-based microcosm experiments.

Percoll Separation

Using a modified protocol from (Orphan et al., 2001a), separation of ANME-SRB consortia from bulk sediment for downstream microscopy or cultivation was performed using a Percoll (Sigma-P1644) density gradient on an aliquot of seep sediment. Cells for microscopy were initially fixed by incubating a 1mL aliquot of sediment with 4% glutaraldehyde overnight at 4˚ C, and were subsequently disaggregated from bulk sediment by sonication for 3 x 10-second intervals on ice using a Branson Sonifier 50 with a power output of 4 W. Cells for downstream sediment-free incubation were not fixed but were also sonicated. A 1 mL aliquot of sonicated sediment was then pipetted onto 500µL of a 100% Percoll density gradient and centrifuged at 18000 x G for 30 minutes at 10˚ C using a Beckman-Coulter Microfuge 18 centrifuge. The supernatant (~1 mL) was then pipetted into 250 mL 1X PBS in a filter tower and vacuumed through a 5 µm polyethersulfone (PES) filter until ~50 mL solution remained in the tower, which was then diluted by ~200 mL 1X PBS added to the tower. Repeated filtration and dilution by 1X PBS was performed 3 times. We calculated this dilution and filtration to remove 99.2% of the 500 µL Percoll (initially containing 0.43 µmol Si (G.E. Healthcare Life Sciences, 2018)) present in the density separation supernatant, with the final filtration step yielding a 1 mL aliquot used for

downstream microscopy. Final [Si] from Percoll was calculated to equal 3.4 μM. Inoculum for the sediment-free incubation experiments was prepared from source sediment using the consortium extraction protocol described above, with the omission of the initial glutaraldehyde fixation step. Percoll separation for sediment-free incubation experiments was performed in a Coy anaerobic chamber with an 97% N_2, 3% H_2 atmosphere.

Bottle Incubations

To enrich for ANME-SRB consortia, seep sediments were homogenized with 0.2 μm filter-sterilized, Ar-sparged deep seawater sampled at to the sampling site and placed in N_2-sparged Pyrex bottles sealed with butyl rubber stoppers. Aliquots from anaerobic Percoll separation to enrich ANME-SRB consortia for sediment-free incubation (see above) were mixed with N_2-sparged artificial seawater (media composition from Scheller, et al. 2016) and placed in N_2-sparged serum vials with butyl rubber stoppers. Carbonate samples were also placed in Pyrex bottles together with filter-sterile N_2-sparged seawater. All incubations were supplied with a CH_4 headspace pressurized to ~2 atm. These anoxic incubations were maintained in the dark at 10˚ C with partial exchange of spent media with the addition of 0.2 μm filter-sterilized Ar-sparged seawater and CH_4 every 3 months. Sediment-free incubations were maintained in these conditions over the course of ~3 years. Sulfate-reducing activity during the course of the incubations was measured using a modified Cline assay (Cline, 1969).

Fluorescence in situ Hybridization and Epifluorescence Microscopy

Conventional fluorescence in situ hybridization (FISH) with a single fluorophore on the 5' end was used to identify ANME-SRB consortia for analysis of consortium exteriors. Here, Percoll-separated AOM consortia were filtered onto 0.2 μm (25 mm) EMD Millipore white polycarbonate filters (Code GTTP) and incubated in 50 μL hybridization buffer for 24 hr at the appropriate formamide stringency, following published protocols (Pernthaler et al., 2001). Percoll separation was only performed on samples from sediment-bearing incubations. Carbonate samples were cut by a rock saw for downstream microscopy. In this study, we used probes targeting Archaea (Arch915; (Stahl and Amann, 1991)), ANME-2 (Eel932; (Boetius et al., 2000)), ANME-2a/b (Treude et al., 2005), and SRB (DSS658; (Boetius et al., 2000)). 4',6-diamino-2-phenylindole (DAPI) was applied as a counterstain, and hybridized samples were illuminated using an XCite Series 120Q fluorescence source and imaged with a Qimage QIClick camera attached to an Olympus BX51 epifluorescence microscope with 60x (Olympus PlanApo N Oil, N.A. 1.42) and 100x (Olympus UPlan FL N Oil, N.A. 1.30) objectives. Imaging software (cellSens Dimension) was used to acquire images. Composites of epifluorescence images were produced using the image processing software Q-Capture Pro 7.

Scanning Electron Microscopy

Scanning electron microscopy (SEM) and energy-dispersive X-ray spectroscopy (EDS) of ANME-SRB consortia from sediment-free incubations immobilized on white

polycarbonate filters or present in situ in carbonate crusts was performed and correlated with optical microscopy. Additionally, sediment samples representing a range of diverse seep sites were filtered onto 0.2 μm EMD Millipore white polycarbonate filters (Code GTTP). Samples were Pd-coated (10 nm thickness) using a Cressington Sputter Coater 208HR and examined using a Zeiss 1550VP Field Emission SEM equipped with an Oxford INCA Energy 300 X-ray EDS system. After SEM image acquisition, EDS mapping of consortia was performed to characterize the spatial distribution of consortium-adhered phases, and EDS point spectra were collected to determine the composition of consortium-adhered phases. EDS data were also collected from non-consortium-associated phases as a comparison. as well as the sediment from which these consortia were separated. SEM images were acquired using an electron beam energy of 10 eV and EDS mapping and spectra were acquired with an electron beam of 15 eV. Subsequent statistical analysis of EDS-acquired compositional data was performed in R.

Transmission Electron Microscopy

ANME-SRB consortia were embedded in Technovit 8200 resin following published protocols (McGlynn et al., 2018), and sectioned using a Leica Ultracut UCT ultramicrotome fitted with a diamond knife. Sections were stained using the contrasting agent osmium tetraoxide and subsequently imaged at UCSD using a FEI Spirit transmission electron microscope operated at 120 kV with a Tietz TemCam F224 2K by 2K CCD camera.

Silicate Grain Size Estimate

TEM micrographs depicting silicates attached to ANME-SRB consortia maintained in sediment-free conditions were processed in Fiji/ImageJ 1.0 to estimate the size distribution of these silicates. A TEM micrograph panorama was constructed using Photoshop from 13 TEM micrographs (20 μm2 each) of a cluster of ANME-SRB consortia. Pixels representing consortium-attached silicates from the TEM micrograph panorama were isolated in Fiji/ImageJ 1.0 by thresholding a grayscale TEM micrograph panorama to only capture pixels of value 0-131 (9.15% of pixels). The thresholded micrograph was further processed using watershed analysis to quantify particle areas in the image with areas 10-1000 μm^2 and circularity 0.5-1. Particle areas were used to estimate particle diameters by assuming the particles approximated spheres, consistent with SEM observations.

The diameter distribution of the 6060 identified particles from the micrograph was used to estimate the true diameter distribution of consortium-attached silicates maintained under sediment-free conditions. A Markov-Chain Monte Carlo approach implemented in MATLAB was used to estimate the true distribution of particle diameters by simulating observed particle diameters produced by random cross-sections of spherical particles assuming a Gaussian size distribution. Particle diameter mean and variance were used as input parameters by the Monte Carlo model which simulated an observed distribution of particle cross-sections and compared these iteratively (10^5 Monte Carlo samples) to the distribution observed via ImageJ in the TEM micrograph panorama. The model converged

on a particle size distribution of maximum likelihood by maximizing the log-likelihood function for the Gaussian distribution.

Focused Ion Beam and Electron Dispersive Spectroscopy

Consortium cross-sections were prepared using a focused Ga^+ ion beam (FEI Nova-600) at the Kavli Nanoscience Institute, Caltech followed by EDS analysis of FIB-sectioned consortia to acquire cross-sectional compositional variability of consortium-attached silicates and consortium interiors.

Inductively Coupled Plasma Mass Spectrometry

[Si] was measured using an Agilent 8800 Triple Quadrupole ICP-MS . A Si standard from Sigma-Aldrich (#15747) was used to calibrate the ICP-MS measurements through a serial dilution procedure. This calibration curve was used to acquire precise measurements for [Si] which were subsequently compared with calculated amorphous silica saturation at temperature and pH conditions corresponding to those of present in sediment-free conditions, using MATLAB and the equations of (Drever, 1988; Gunnarsson and Arnórsson, 2000). Additionally, [Si] was compared to experimentally-determined equilibria describing adsorption of Si to various aluminosilicate clays (Siever and Woodford, 1973).

Comparative Genomics

To explore potential mechanisms for mediation of silicate precipitation by members of ANME-SRB consortia, metagenomes acquired from ANME-SRB consortia (Skennerton et al., 2017) were used as a database to search for predicted proteins possibly involved in condensation of orthosilicic acid to form the observed precipitate attached to ANME-SRB consortia. An approach similar to that of (Scheffel et al., 2011) was used, in which a metagenomic database is searched for predicted proteins possessing a sequence of amino acids with residue frequencies suggestive of involvement in orthosilicic acid condensation. Here, the python module biopython (Cock et al., 2009) was used to parse a metagenomic database for proteins containing ≥ 25% serine and ≥ 20% lysine or arginine residues in a sliding 30 amino-acid-long window, a criterion inspired by the amino acid composition of a spore coat protein from *Bacillus cereus* known to be involved in silica precipitation (Motomura et al., 2016). Candidate proteins selected by this criterion were then further filtered using BLASTp for extracellular membrane-associated proteins. PSORTb 3.0 (Yu et al., 2010) was used to predict signal peptide sequences in candidate proteins.

RESULTS

FISH-EM Imaging Reveals Silicates Attached to ANME-SRB Consortia

Correlated epifluorescence microscopy, SEM, and elemental mapping via EDS (Figs. 1, S1) documented the presence of silicate phases on the exteriors of ANME-SRB

consortia extracted directly from methane seep sediment samples (Fig. 1A-C) and additionally revealed the presence of silicates distributed between consortia grown under sediment-free conditions (Fig. 1D-O). Silicates appearing on consortia extracted directly from sediments collected from seafloor methane seep sites of the Santa Monica Basin (Fig. 1B) were often difficult to distinguish under SEM from C-rich domains but were apparent when elemental maps documenting the spatial distribution of C and Si were constructed (Fig. 1C). Si-rich domains attached to ANME-SRB consortia extracted from methane seep sediment samples appeared as massive phases intergrown with consortium exteriors (Fig. 1B). Occasionally, Fe- and S-rich domains with framboidal textures (putative pyrite) appeared embedded in Si-rich domains (Fig. 1C).

AOM-active ANME-SRB consortia maintained in the laboratory for 3 years under sediment-free conditions harbored biomass consisting of multiple clusters of ANME-SRB consortia within EPS matrix (Figs. 1D-O, S1). Correlated epifluorescence FISH microscopy and SEM-EDS revealed these intergrown cell clusters were embedded in a matrix containing Si-rich phases and C (Figs. 1G-N, S1). These silicate phases were attached to the exteriors of consortia and differed in appearance from those observed on consortia sampled directly from sediment in their botryoidal habit, appearing as ~200 nm spheres forming intergrown Si-rich masses (Figs. 1G-N). These masses display a range of textural attributes, encrusting consortium exteriors (Fig. 2A,C), grading into smoother features of lower porosity (Fig. 2A,B), occasionally hosting framboidal Fe- and S-rich phases (Fig. 1N,O), and nearly or entirely enveloping consortia (Figs. 2A, S1H).

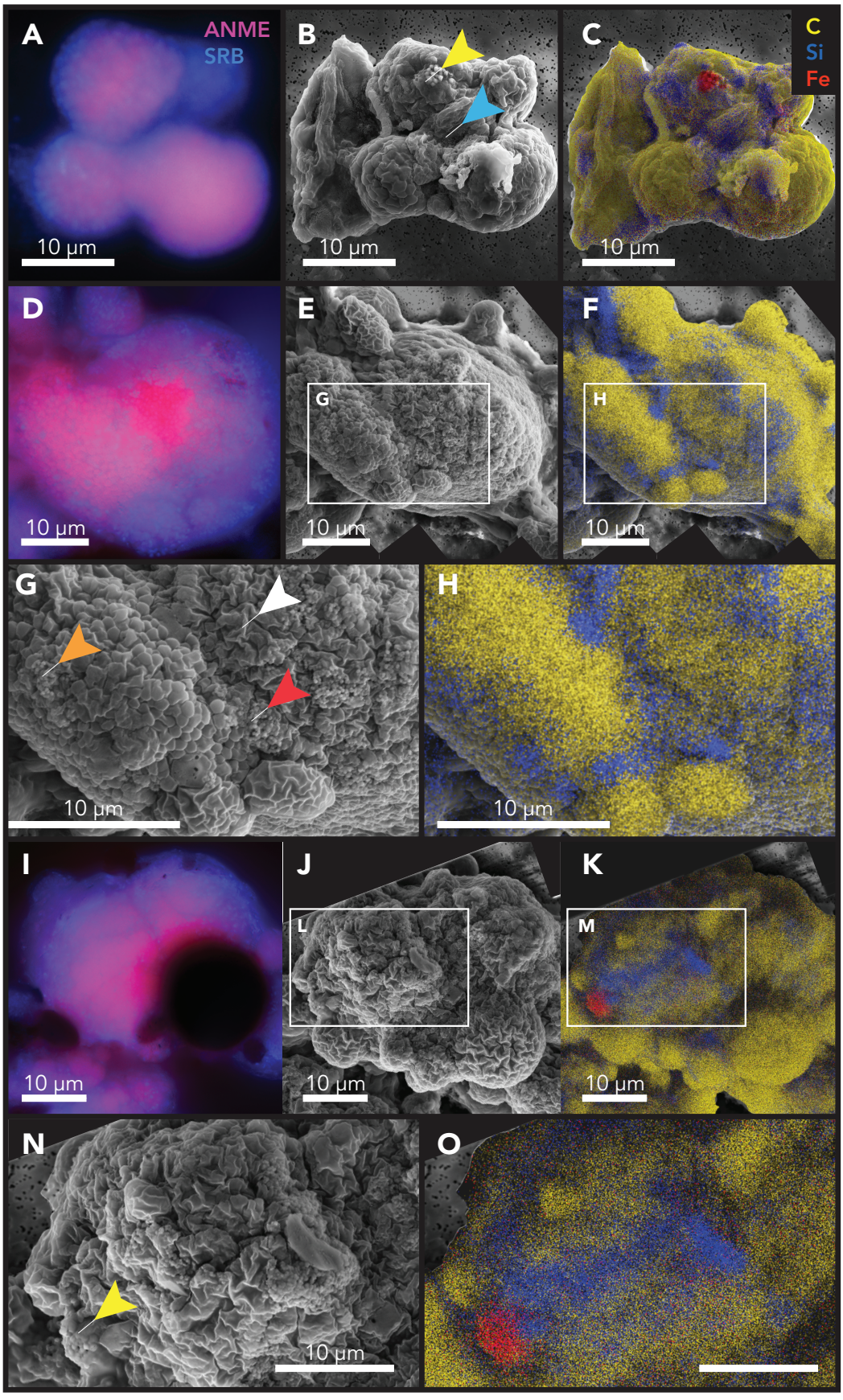
A
ANME
SRB
10 µm
B
10 µm
C
C
Si
Fe
10 µm
D
10 µm
E
G
10 µm
F
H
10 µm
G
10 µm
H
10 µm
I
10 µm
J
L
10 µm
K
M
10 µm
N
10 µm
O

Figure 1. Correlated epifluorescence (using FISH; A,D,I), SEM (B,E,G,J,N), and EDS (C,F,H,K,M) images documenting the presence of silicate phases attached to ANME-SRB consortium exteriors extracted from methane seep sediments from Santa Monica Basin (A-C), or from sediment-free AOM consortia incubations (D-O). In ANME-SRB consortia extracted directly from methane seep sediment samples, Si-rich domains between consortia are intergrown with consortia exteriors (B, *blue arrow*). In the sediment-free incubation, silicates are present between consortia which appear as clusters of dozens of ANME-SRB consortia, and have botryoidal, authigenic textures (G, *red arrow*) and encrust ANME exteriors (G, *orange arrow*). These botryoidal silicates were distinguishable from the rugose, C-rich consortium exteriors (*white arrow*) they encrust. Additionally, Fe- and S- rich domains observed via EDS (C, O) correlate with framboidal textures observed in SEM imagery (B, N, *yellow arrows*).

An ultrathin section of consortia biomass imaged by TEM (Fig. 2D) further revealed the textural characteristics of Si-rich phases with a particle size distribution of 230±62 nm (n = 6060) by image processing and Monte Carlo simulations. These sub-micron scale Si spheres were localized between multiple ANME-SRB consortia, embedded in the less coherent mineral-organic matrix adhering consortia to each other in a larger (~200 μm) biofilm.

Silicate Composition via EDS and FIB-EDS

EDS was used to compare the elemental composition of consortium-attached phases to free silicate phases (predominantly, clay particles) in the sediments from which ANME-SRB consortia were extracted. Elemental compositions, reported as weight percent of each element, were converted to atom percent to aid in phase identification. Phases attached to consortia extracted from both sediment-containing and sediment-free incubations are typically ~5-20 atom % Si, ~0-5% Al, and ~0-5% Fe (Fig. S2), but the raw atom % calculated from EDS data underrepresents Si, Al, and Fe due to high C and O

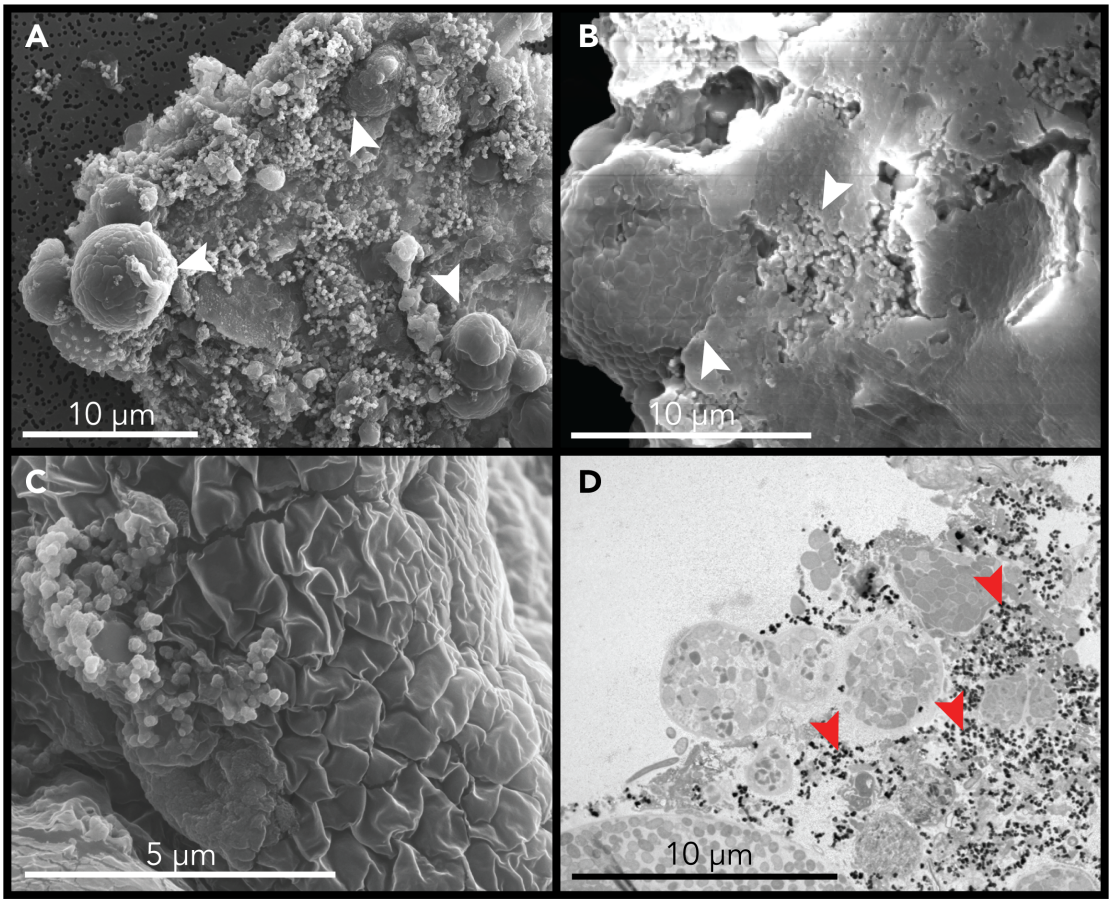

Figure 2. SEM imagery documenting the texture of silicate phases attached to ANME-SRB consortia grown under sediment-free conditions reveals the common appearance of these phases as ~200 nm botryoidal subspherical particles intergrown (A-B, *white arrows*) and encrusting consortia (A,C, *white arrows*). TEM imagery of a cross-section of a consortium cluster (D) demonstrates the distribution of this phase between consortia (*red arrows*), allowing for a quantitative estimation of sphere particle size (230±62 nm; Fig. S7).

signal from the associated biomass. To reduce this analytical bias, the data were analyzed as elemental ratios (atom % per atom %) which are unbiased by an abundance of C or O due to proximity to biomass (Fig. 3). The ratio of elements typically found in octahedral sites (Mg + Al + Fe) of clays to Si was also calculated, and revealed most consortium-attached phases to have more than 2 Si per octahedral cation. A one-way ANOVA test determined the elemental ratios between consortium-attached phases and the sediment

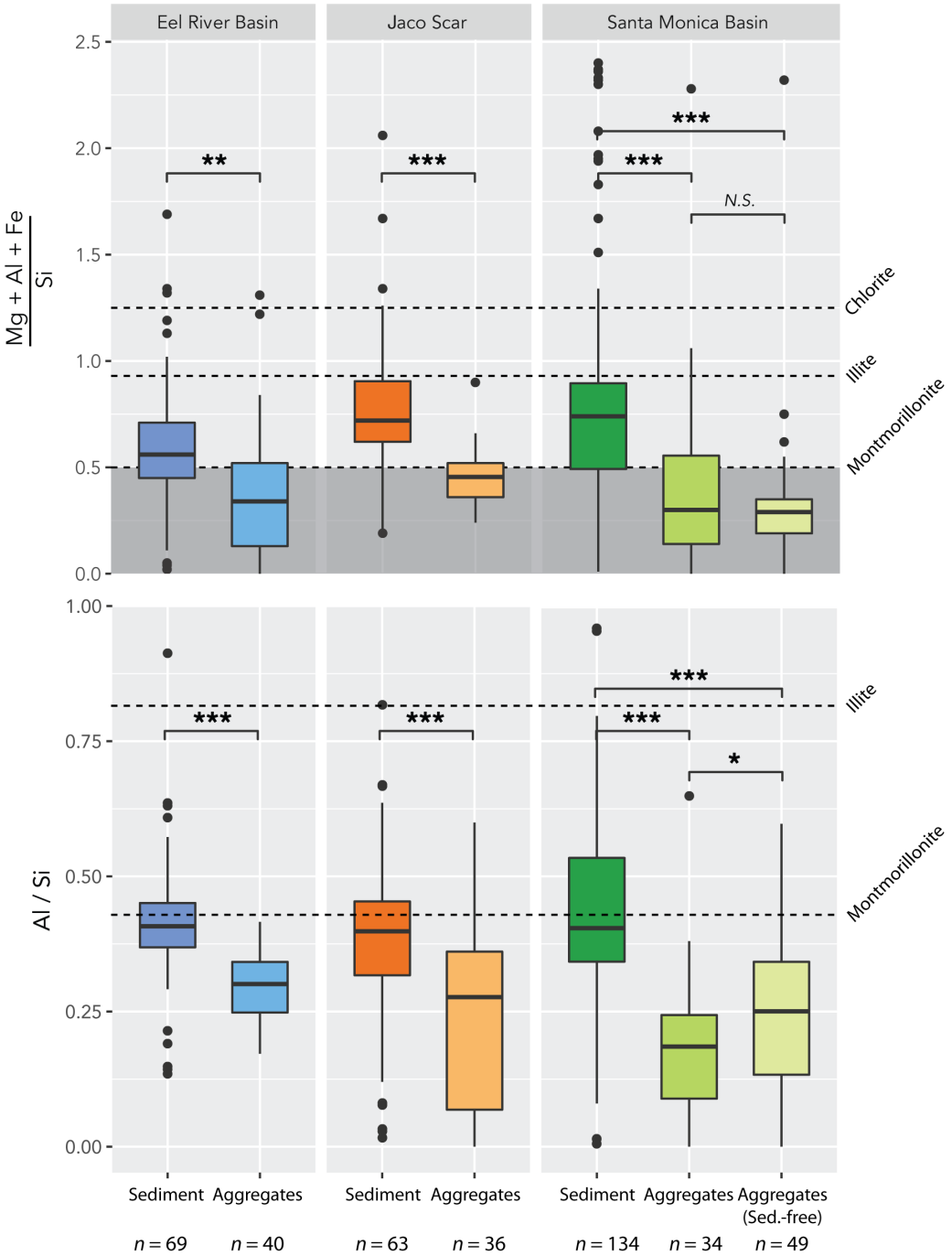

Figure 3. EDS-acquired compositional data of ANME-SRB consortium-attached silicates extracted directly from sediments or grown under sediment-free conditions compared with the range of compositions of silicates in the sediment from which the samples were drawn demonstrates the statistical significance (One-way ANOVA test, ***: $p<0.001$, **: $p<0.01$, *: $p<0.05$, *N.S.*: $p>0.05$) of compositional differences between consortium-attached silicates and source sediment due to significant Si enrichment in consortium-attached silicates. This enrichment is incompatible with the precipitation of stoichiometric clay, shown in the upper panel, which should have an octahedral cation : Si ratio greater than 0.5. Reference ideal clay mineral compositions taken from (Moore and Reynolds, 1997); chlorite omitted from bottom panel as ideal chlorite Al/Si ≥ 1.25.

samples from which consortia were extracted were all statistically significant in all samples (Fig. 3). Notable, elemental compositions of phases attached to consortia grown under sediment-free conditions (originally extracted from Santa Monica Basin methane seep sediments) were compositionally similar to those found attached to consortia recovered directly from those sediments by several elemental ratios ($p > 0.05$).

Using a focused ion beam (FIB), a cross-section through the center of a FISH-identified ANME-2—DSS consortium was prepared and subsequently analyzed by EDS. Data showed organic-rich interior with abundant C and N, with a Si-enriched phase on consortia exteriors in cross-section (Fig. 4). Si, Al, and Fe atom % measurements on the consortium exterior are comparable to those measured in non-sectioned consortia. Additionally, (Mg + Al + Fe) : Si measured on silicates attached to the FIB-sectioned consortium were similar to the measurements of this ratio on non-sectioned consortia, ranging between 0.25-0.29, or greater than 4 Si per octahedral cation.

ICP-MS

Si concentrations in the seawater media from the sediment-free incubations were low (1.22 ± 0.19 μM), as measured by ICP-MS (Fig. S5). Calculations of silica solubility at the pH (buffered to pH 8) and temperature (10˚ C) conditions present in sediment-free incubations demonstrated the sediment-free incubation media to be significantly undersaturated with respect to amorphous silica and equilibrium adsorption of Si to clay minerals.

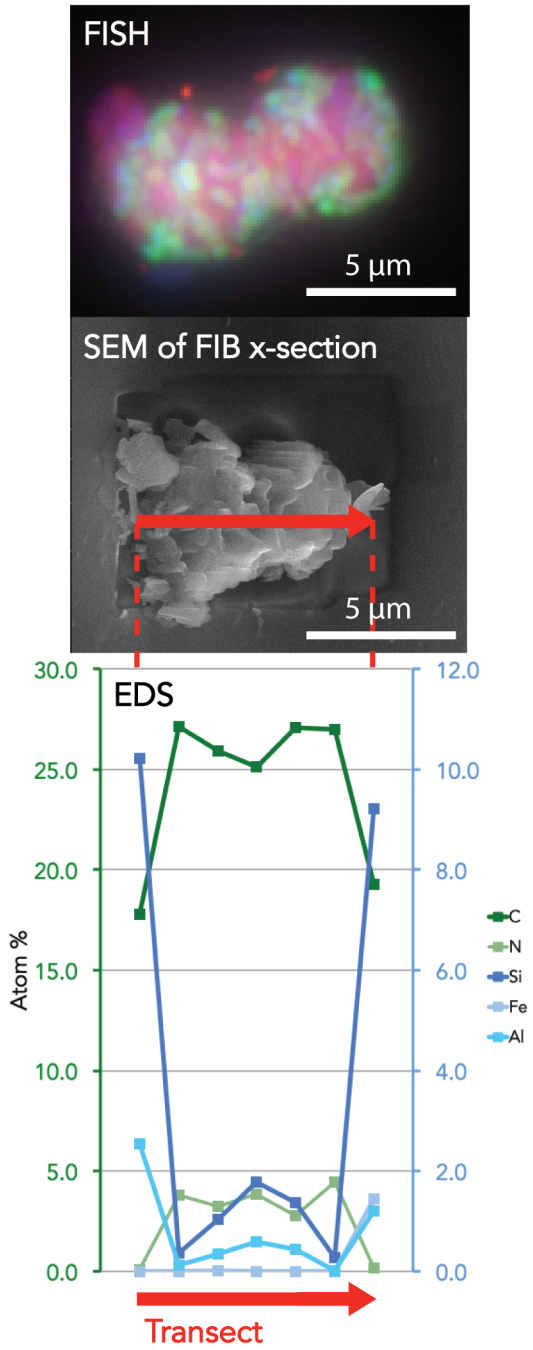

Figure 4. Correlated FISH and SEM micrographs of an ANME-SRB consortium (ANME-2, pink, stained by probe Eel 932; SRB, green, probe DSS 658) sectioned subsequent to epifluorescence microscopy by Ga^{+} FIB (after Dekas, 2013). Chemical analysis of a transect of this cross-section reveals consortium-attached silicate compositions similar to those measured on non-sectioned consortia, with Si enrichment relative to the source sediment inconsistent with stoichiometric clay compositions (octahedral cation : Si ≈ 1 : 4).

Seep Carbonates Contain C-rich Domains with Si-rich Margins

Epifluorescence microscopy and SEM imaging of a sample of seep carbonate recorded ~10-20 μm diameter aggregates of cocci stained by DAPI (Fig. 5A). FISH hybridization of these aggregates failed, potentially due to high background fluorescence from the carbonate matrix. These aggregates were common in the carbonate matrix, appearing particularly concentrated near or in vugs, cracks, or other porous features within the seep carbonate. These aggregates displayed a similar morphology to one another, with a bimodal distribution of cell sizes, larger cells located in the center of aggregates, and smaller cells near aggregate margins. SEM imaging of this seep carbonate sample documented electron-dense domains with similar morphology and spatial distribution to that observed for the DAPI-stained aggregates (Fig. 5B), although correlated fluorescence microscopy and SEM was not performed. EDS analysis of these electron-dense domains revealed them to be more C-rich than the carbonate matrix, and also surrounded by elevated Si concentrations (Fig. 5C-E).

Community Analysis

To determine the microbial community composition in the Si precipitating-AOM incubations, 16S rRNA amplicon sequencing was performed. 16S rRNA amplicon sequencing data from the sediment-free AOM incubation after 3 years of enrichment revealed a high proportion of reads (OTUs clustered at a 97% similarity) affiliated with ANME-2a/b (40% of total reads) and previously-established partner organism SEEP-SRB1

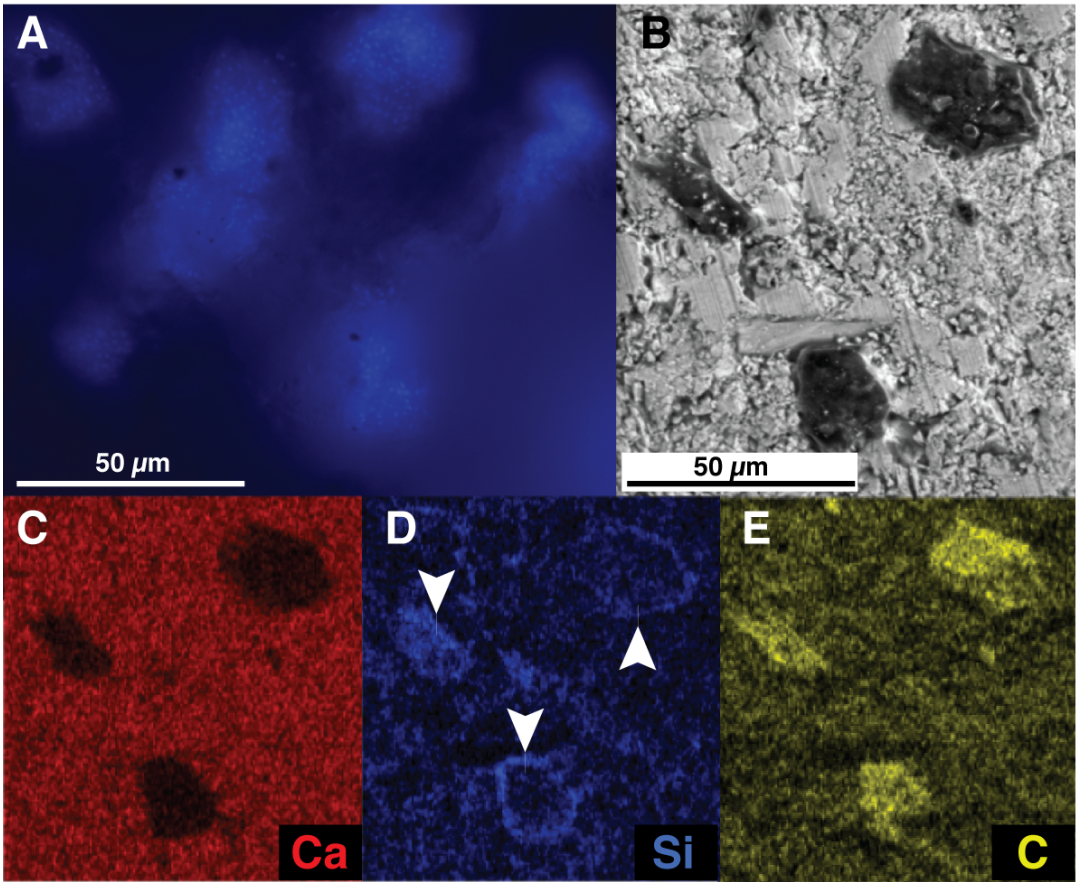

Figure 5. Epifluorescence microscopy (A) and SEM-EDS (B-E) imaging of putative ANME-SRB consortia embedded in seep carbonate. Microscopy (A) revealed the presence of many DAPI-stained microbial aggregates with morphology highly similar to that previously observed for ANME-SRB consortia embedded in carbonate (cf. Marlow, et al. 2014). SEM imaging of this seep carbonate sample documented the presence of several electron-dense (B) domains of similar size, morphology, and distribution as those of putative ANME-SRB consortia as observed by epifluorescence microscopy, although direct correlative imaging was not performed. EDS mapping of these putative ANME-SRB consortia revealed high Si concentrations localized to the exterior of these putative consortia (D, *white arrows*).

(15%; Figure S6). Other SRB detected in these incubations include SEEP-SRB2 (0.7% of total reads) and Desulfobacula (0.8% of total reads). While ANME-2a/b were the dominant archaeal group detected, minor contributions from methanogenic Methanococcoides (2% of archaeal reads) and from members of the class Thermoplasmata (6% of archaeal reads)

were also detected, while bacterial lineages associated with the the Chloroflexi (1% of total reads), heterortophic MBGD, and the Planctomycetes (2% of total reads).

Comparative Genomics

A search for predicted proteins containing serine- and lysine-/arginine-rich sequences was performed using a database of ANME and SRB genomes, followed by a search for similar proteins using BLASTp. The first part of the search was implemented in Python, using a sliding window of variable size to search for domains of any given ORF within the genome with a count of serine, lysine, and/or arginine residues within this window above a threshold. Of many candidate proteins uncovered during this search process, one predicted protein (NCBI Accession OEU44463) associated with metagenome-assembled genome bin from Santa Monica Basin (Desulfobacterales sp. S7086C20 (Skennerton et al., 2017)) affiliated with the SEEP-SRB1, clade of sulfate-reducing partners of ANME (Schreiber et al., 2010; Skennerton et al., 2017) with a particularly serine- and arginine-rich C-terminal sequence was found. Further analysis via BLAST revealed the identity of this protein as a member of the DUF3300 family of hypothetical membrane proteins, and was also predicted by PSORTb 3.0 (Yu et al., 2010) to have a signal peptide suggesting extracellular localization.

DISCUSSION

Previous research documented the presence of silicates with authigenic textures on the exterior of ANME-SRB consortia (Dekas, 2013; Chen, et al., 2014), but it was not clear to what extent these phases represented the product of active microbially-mediated precipitation as has been suggested, rather than passive attachment of silicates to ANME-SRB consortia by abiotic processes. To investigate this, we examined silicates attached to the exterior of ANME-SRB consortia grown under sediment-free conditions and compared these phases with those attached to ANME-SRB consortia extracted from methane seep sediments. Correlated epifluorescence microscopy and SEM-EDS imaging revealed the presence associated with Si-rich phases on ANME-SRB consortia (Fig. 1). These phases appeared intimately associated with consortium exteriors, sometimes intergrown with a C-rich matrix between consortia interpreted extracellular polymers. EDS-acquired compositional data of these Si-rich phases display compositions consistent with the interpretation of these phases as a silicate precipitate. Notably, consortium-attached silicates differ significantly (one-way ANOVA test, $p < 0.01$) from the composition of detrital silicates in the sediments from which they were sourced (Fig. 3) due to the Si-enriched nature of the consortium-attached silicates. When the elemental composition of consortium-attached silicates was examined using the ratio of elements typically found in octahedral sites of clay minerals (Mg, Al, Fe) to Si, it is clear that a majority of consortium-attached silicates are more enriched in Si than known clay mineral compositions. The most Si-rich clay possible (e.g. montmorillonite, $(Na,Ca)_{0.33}(Al, Mg)_2(Si_4O_{10})(OH)_2 \cdot nH_2O$), in which the ratio of tetrahedral to octahedral sheets is 2:1 and Si occupies all tetrahedral sites, could only have a octahedral cation to Si ratio of 0.5 (Moore and Reynolds, 1997);

however, most consortium-attached silicates have octahedral cation: Si ratios < 0.5 (0.40 ± 0.39, Fig. 3). In contrast, most compositional measurements of terrigenous detrital silicates in methane seep sediment samples from which consortia were extracted have octahedral cation : Si ratios of ~0.75 (0.82 ± 0.51), consistent with clay minerals. Notably, the silicates attached to ANME-SRB consortia from our work are significantly more Si-rich than cell-attached silicates previously used as a model for silicate precipitation aided by Fe or Al adsorption on cell walls ((Konhauser and Urrutia, 1999); Fig. S3). EDS performed along a transect of a FIB-sectioned ANME-SRB consortium corroborated observations of silicates attached to intact consortia recovered directly from seep sediments (Fig. 4). EDS elemental analysis along the transect supports the presence of silicates attached to external surfaces, as Si enrichment at consortium edges transitions to C and N-rich domains toward consortium interiors.

These observations, consistent with previous study of silicate phases attached to ANME-SRB exteriors, demonstrate to a high degree of statistical significance that ANME-SRB consortia extracted directly from seep sediments recruit Si to consortium exteriors, producing authigenic Si-rich silicate precipitates significantly Si-enriched relative to the silicates present in their host sediment. The Si-rich compositions of these phases stand in contrast to silicates observed attached to microbial exteriors in previous experiments in which Fe or Al adsorption to cell surfaces recruits Si from solutions rich in dissolved Si (≥150 μM), producing Fe- and/or Al-rich phases (Fig. S3 (Ferris et al., 1987; Konhauser et al., 1993, 1994; Mera and Beveridge, 1993; Köhler et al., 1994, 1999; Urrutia and Beveridge, 1994; Konhauser and Urrutia, 1999; Fein et al., 2002)). Previous work

describing ANME-SRB consortium-attached silicates, postulated a role for Al adsorption to ANME-SRB cell exteriors in mediating silicate precipitation (Chen et al., 2014), a mechanism which has only been shown to produce Fe- and/or Al-rich phases attached to cell exteriors (Urrutia and Beveridge, 1994; Konhauser and Urrutia, 1999). Additionally, Al-adsorption to cell exteriors has only been demonstrated to interact with silicate precipitation in media with sufficient dissolved Si ([Si] ≥ 150 μM) to drive abiotic silicate precipitation, obscuring the degree of biologically-mediated silicate precipitation (Urrutia and Beveridge, 1994; Konhauser and Urrutia, 1999). The significant compositional difference between Si-rich silicates observed here attached to ANME-SRB consortia and that of cell-attached silicates produced by interactions between Fe and/or Al adsorbed to cell surfaces (Fig. S3; (Konhauser and Urrutia, 1999)) suggests other processes may be involved in the precipitation of Si-rich silicates on ANME-SRB consortium exteriors. However, the degree to which silicate precipitation onto ANME-SRB consortia sourced directly from sediments is biologically controlled was difficult to assess without additional constraints on porewater geochemistry, as sufficiently high [Si] could possibly catalyze abiotic precipitation of authigenic silicates. Previous observations of ANME-SRB consortium-attached silicates from the South China Sea (Chen et al., 2014) were collected from incubation samples with no constraints on porewater [Si] (Zhang et al., 2010, 2011).

We were able to test the hypothesis that ANME-SRB consortia are capable of removing Si preferentially from solution, producing Si-rich silicate precipitates on consortium exteriors by analyzing a sediment-free incubation of ANME-2b—DSS consortia anaerobically prepared from methane seep sediments of Santa Monica Basin

using Percoll-based density separation. After 3 years of sediment-free incubation under AOM conditions enriching for the growth of ANME-SRB consortia, correlated epifluorescence microscopy and SEM-EDS analysis documented large clusters consisting of dozens of ANME-SRB consortia embedded in a Si-rich matrix that, under SEM, consisted of ~200 nm Si spheres intergrown with rugose, C-rich domains interpreted as EPS (Figs. 1G,H, 1N,O, 2A-C, S1). Occasionally, framboidal Fe- and S-rich domains were observed in this matrix, likely framboidal pyrite or other iron sulfide phases produced during active, sulfate-coupled AOM. The growth habit of clusters of many AOM consortia held together by a mineral-organic matrix contrasts with the appearance of consortia extracted directly from sediment by standard sonication- and density separation-based techniques, the latter typically appearing in epifluorescence microscopy as single consortia of 50-5000 cells (Boetius et al., 2000; Orphan et al., 2001b, 2002). Notably, the polyconsortium clusters observed here (Figs. 1D-O, 2, S1, S4), sourced from sediment-free incubations were observed without the sonication, density separation, and filtration steps necessary to extract consortia directly from sediment, steps that may bias observations against such clusters in situ. TEM observations of consortia grown under sediment-free conditions corroborated SEM-EDS images, revealing the presence of abundant 230±62 nm-diameter subspherical particles between consortia, and confirming the presence of these silicate phases throughout consortium clusters (Fig. 2D). We were initially concerned that some portion of these phases may represent Percoll contamination, but calculations based on the abundance of consortium-attached silicates and estimated total ANME-SRB biomass in these incubations precluded the introduced Si from Percoll as a sufficient source of Si for the consortium-attached silicates. Additionally, the size distribution of these subspherical

silicate particles eliminates the possibility of significant Percoll contamination which is represented by colloidal silica particles of diameter 15-30 nm (G.E. Healthcare Life Sciences, 2018).

Observations of silicates distributed between consortia grown under sediment-free conditions are consistent with previous observations (Chen et al., 2014), which were collected from consortia sampled directly out of sediment without use of Percoll density separation, suggesting this silicate precipitation to be a biological phenomenon of ANME-SRB consortia, rather than an artifact of the consortia enrichment procedure. We further analyzed the process of silicate precipitation by ANME-SRB consortia using a model describing growth of consortia within EPS using consortium doubling times of 3-9 months taken from the literature (Girguis et al., 2005; Nauhaus et al., 2007; Dekas et al., 2009; Meulepas et al., 2009; Orphan et al., 2009). Assuming consortia clusters observed after 3 years of incubation had increased exponentially from a small number of starting consortia, the consortium counts in a larger cluster from epifluorescence data (Fig. S4) were used to constrain the maximum number of consortia present at $t = 0$ that could have produced the observed consortium number after 3 years of incubation (Fig. 6). The model demonstrates that significant consortium growth over 3 years is required for even the longest generation times (9 months). Therefore, the Si-rich phases observed in the extracellular matrix between consortia must have developed subsequent to inoculation, as the majority of consortia embedded within these phases are required by reasonable doubling times to have grown subsequent to inoculation. Measurement of [Si] in sediment-free incubation media post-incubation via ICP-MS, 1.2 ± 0.2 μM, precluded abiotic mechanisms of Si enrichment

of consortium-attached silicates, as a [Si] of 1.2 µM was below concentrations previously reported to drive was too low to drive either amorphous silica precipitation (~1000 µM) or Si adsorption on pre-existing consortium-attached silicates (≥200 µM (Siever and Woodford, 1973); Fig. S5). Silicon concentrations in sediment-free incubations are also inconsistent with silicate precipitation associated with the initial gradient separation, as such precipitation again would only occur with Percoll-introduced [Si] above Si clay adsorption equilibria (Siever and Woodford, 1973), far above the ~3 µM of Percoll-associated [Si] estimated to be introduced during the initial gradient separation.

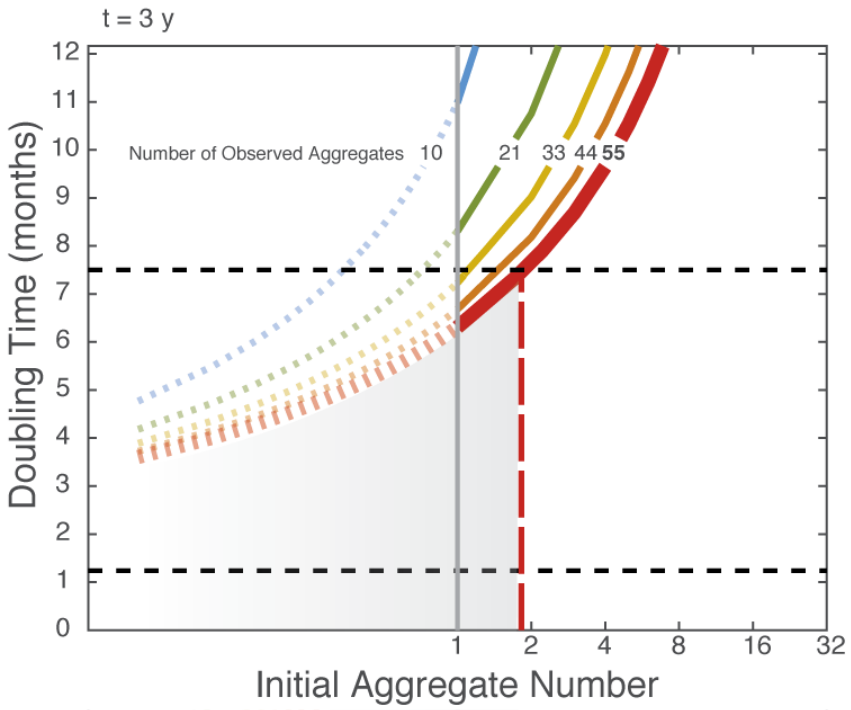

Figure 6. A model calculating initial ANME-SRB consortium number required to produce a given number of consortia observed after 3 years of sediment-free incubation indicates that for previously-calculated consortium doubling times (Girguis et al., 2005; Meulepas et al., 2009; Nauhaus et al., 2007), even the largest consortium clusters must have grown from a small percentage of their current number, assuming consortia observed in a cluster grew from a smaller number of consortia. Thus, silicates observed between consortia must have grown subsequent to inoculation, from media undersaturated with respect to amorphous silica and Si adsorption on aluminosilicate clays (S5).

Together, these lines of evidence disprove the null hypothesis that consortium-attached silicates formed due to passive attachment of detrital silicates on ANME-SRB consortium surfaces or via known mechanisms of abiotic silicate precipitation from solution, implying active local removal of Si from solution during AOM by ANME-2—SRB consortia and suggestive of bona fide silicate biomineralization by ANME-SRB.

The biological mechanism used by ANME-SRB consortia to catalyze orthosilicic acid condensation is currently unknown. Prokaryotic silicate biomineralization of Si-rich phases in undersaturated conditions has been previously observed in experiments examining the Si-bearing spore coat of the *Bacillus subtilis* (Motomura et al., 2016). In this gram-positive bacterium, condensation of dissolved orthosilicic acid was demonstrated to be catalyzed by a particularly serine- and arginine- rich sequence of a spore coat protein (Motomura et al., 2016). The zwitterionic nature of this sequence is similar to that of silacidins and silaffins, proteins that contribute to silica precipitation in diatoms serine- and lysine-rich proteins thought to contribute to silica precipitation in diatoms (Kroger et al., 2001; Wenzl et al., 2008; Richthammer et al., 2011). Following previous work attempting to find silaffin-like proteins in diatom genomes (Scheffel et al., 2011), we performed a search through our seep metagenome database to find proteins with similar, C-terminal zwitterionic sequences rich in serine and lysine or arginine residues. One serine- and arginine-rich hypothetical protein was found in association with a Deltaproteobacteria (SEEP-SRB1) partner of ANME (Desulfobacterales sp. S7086C20, NCBI accession OEU44463; (Skennerton et al., 2017)) predicted to be membrane-associated and localized to the cell surface. Additional support for the extracellular localization of this protein was

suggested by the prediction of a hydrophobic DUF3300 domain in the protein. Related proteins with serine- and lysine/arginine-rich C-terminal sequences were also detected in other Desulfobacterales (Desulfobacterales bacterium SG8_35_2, NCBI accession KPK26241.1) and additional members of the Deltaproteobacteria, including *Geobacter uraniireducens* Rf4 (NCBI accession WP_011939518.1) may be candidates for investigating the degree to which this group of membrane proteins may be involved in silicate biomineralization via interactions between its C-terminal zwitterionic sequence and dissolved orthosilicic acid.

Another notable example of prokaryotic silicate biomineralization with potential relevance to the ANME-SRB syntrophy is the potential link between extracellular Fe reduction of iron-rich clays and concomitant silica precipitation. Observations of silica precipitation in media undersaturated with respect to amorphous silica were reported from experiments in which silica precipitation occurred during the reductive dissolution of Fe-rich clay minerals by iron- and sulfate-reducing bacteria (Dong et al., 2003; Li et al., 2004; O'Reilly et al., 2005; Furukawa and O'Reilly, 2007; Zhang et al., 2007) (Li et al., 2004). Here, silica precipitation was proposed to occur through the activity of polyamines, long-chain forms of which (>7 aminopropyl units) have been proposed to play an important role in silica precipitation in diatoms (Kröger et al., 2000; Belton et al., 2008) and have been shown to precipitate silica in undersaturated conditions from silica oligomers (Patwardhan et al., 2011). Long-chain polyamines, structurally-similar to thermospermine (Kröger et al., 2000), have been proposed to be synthesized in diatoms by aminopropyl transferases with a conserved GGGE motif (Michael, 2011). Prokaryotic aminopropyl transferases with a

conserved GGGE motif related to those in diatoms (Minguet et al., 2008) also produce longer-chain and branched polyamines >4 aminopropyl units long (Hamana et al., 1991; Knott, 2009; Ohnuma et al., 2011). We searched existing ANME-SRB metagenome data for aminopropyl transferases homologous to those known to produce long-chain polyamines. However, no ANME or SRB genome contained homologous aminopropyl transferases; the only homologous sequence was an aminopropyl transferase from a reconstructed Dehalococcoides from methane seeps.

Although the biochemical mechanism catalyzing silicate precipitation mediated by ANME-SRB remains uncertain, observations of silica precipitation resulting from interactions between Fe- or sulfate-reducing prokaryotes and clays may give insight into possible sources of Si precipitated in phases attached to consortium surfaces. Recent evidence strongly suggests ANME performs direct electron transfer to SRB partners through multiheme cytochrome complexes (McGlynn et al., 2015; Wegener et al., 2015), and ANME have been shown to use insoluble Fe, Mn oxides and soluble electron shuttles as electron acceptors (Beal et al., 2009; Sivan et al., 2014; Ettwig et al., 2016; Scheller et al., 2016; Leu et al., 2020). These extracellular electron transfer models of ANME-SRB syntrophy are similar to direct electron transfer by organisms such as *Shewanella oneidensis* and *Geobacter* sp. shown to be capable of reducing clay-bound iron with concomitant removal of Si from clays, driving silicate precipitation in undersaturated conditions as discussed above (Dong et al., 2003; O'Reilly et al., 2005; Furukawa and O'Reilly, 2007; Zhang et al., 2007). The poorly-understood process of silica precipitation occurring as a result of clay interactions with various Fe- and sulfate-reducers could

possibly explain observations of consortium-attached silicates and iron sulfide: silicate precipitation could be driven by auxiliary Fe-reduction of clay-bound Fe by consortia, either by direct transfer of electrons by protein complexes or redox-active shuttles to clays adhered to consortium exteriors or through indirect reduction via sulfide oxidation. However, silica precipitation driven by clay dissolution alone would imply by mass balance the presence of an equally-abundant Al-enriched clay residue in our experiments. While we do not observe such phases attached to ANME-SRB consortium clusters in our experiments, previous study of the mineral products of dissimilatory reduction of iron-bearing clay minerals (O'Reilly et al., 2005) as well as previous study of the mineralogy of silicates attached to ANME-SRB consortia (Chen, et al 2014) documented such Al-rich residues, which in the latter study were identified by TEM as Al-rich silicate crystals of kaolinite and/or nacrite (both $Al_2Si_2O_5(OH)_4$). Future work is necessary to parse the extent of direct silica precipitation from media vs. precipitation via proximal clay dissolution, as this will help resolve these competing hypotheses.

The presence of silicate phases precipitated on consortium surfaces and between consortia suggests the purpose of these phases may be to give structure to consortium exteriors or to polyconsortium clusters as those observed here in sediment-free incubations. If these polyconsortium clusters exist as a major mode of consortium growth in vivo, authigenic silicates may ensure the ability for consortia to share resources, as has been observed within consortia for N_2-fixation (Dekas et al., 2009; Dekas et al. 2016; this thesis, Chapter 1). It remains unknown, however, if the cluster mode of consortium growth is

present in environmental settings; examining positions of consortia directly within the sediment matrix is a promising direction of future research.

The mode of prokaryotic silicate biomineralization described in this study may be additionally important for the preservation of organic carbon in the rock record. Authigenic silicates are well-known to provide excellent preservation potential in rocks of all ages, providing early occlusion of pore space which protects organics from degradation (Callow and Brasier, 2009; Newman et al., 2016). Early silicate cements are important in fossil seep carbonates spanning the Phanerozoic, where silica appears as fibrous and botryoidal cements replacing aragonite or cryptocrystalline void-filling cements (Peckmann et al., 2002; Himmler et al., 2008; Kaim et al., 2008; Kuechler et al., 2012; Smrzka et al., 2015; Miyajima et al., 2016). Early silica precipitation in seep carbonates can entomb organics; in one striking example, preservation of vestimentiferan tube worm chitin by early silicate cements in Late Cretaceous (Campanian) seep carbonates of Japan has been documented (Hikida et al., 2003). In rare cases, silicate cements from both fossil (Miyajima et al., 2016) and modern (Köhler et al., 1999) seep carbonates have even been observed to trap CH_4 in hydrate minerals, suggesting silicate cementation concomitant with CH_4 production (Lazzeri et al., 2017).

Here, we document in seep carbonate samples the presence of Si-rich phases localized to the margins of C-rich domains (Fig. 5). Although we could not exactly correlate these features between SEM and epifluorescent microscopy, these C-rich domains share morphology and spatial distribution with those of DAPI-stained aggregates with morphology suggestive of ANME-SRB consortia (Fig. 5A). On the basis of these

observations, we hypothesized that these domains represent ANME-SRB consortia that precipitated silicates on consortium exteriors. We further speculated that the precipitation of silicates on the exteriors of these putative ANME-SRB consortia served to preserve their biomass. Our hypothesis could be tested by measurement of the carbon isotope compositions of these domains by SIMS. If this hypothesis is confirmed, these features would then present a useful search image for ANME-SRB consortia preserved in fossil seep carbonates.

The importance of early silicate cementation in seep carbonates and in siliciclastic sediments more broadly (Newman et al., 2016) for non-mineralized tissue preservation in the rock record raises the question of the degree to which understudied prokaryotic silicate biomineralization may interact with this process. Silica-precipitating diatom silaffin sequences are highly divergent, implying the evolution of zwitterionic peptides as a method for biological control of silicate mineralization to have occurred multiple times, further demonstrated by the silicate-precipitation activity of a *Bacillus subtilis* spore coat protein (Kroger et al., 2001; Scheffel et al., 2011; Motomura et al., 2016). The possibility that similar convergent evolution may have produced a variety of yet-uncharacterized proteins similar to that discussed here from Desulfobacterales sp. S7086C20 motivates future work to directly test the degree to which this protein can catalyze silicate precipitation in solutions undersaturated with respect to amorphous silica. A demonstration of silicate precipitation in undersaturated conditions catalyzed by this protein would be an important step in improving our understanding of biological mediation of early silicate cementation in the rock record.

CONCLUSIONS

We demonstrate here for silicate precipitation in undersaturated and sediment-free media within the extracellular matrix produced by ANME-SRB consortia. SEM-EDS examination reveals this silicate phases to exhibit authigenic textures similar to those observed on the exteriors of ANME-SRB consortia removed directly from sediment, suggesting that silicates precipitated on the exteriors ANME-SRB consortia grown under sediment-free incubations are representative of those previously discussed in the literature. Additionally, the composition of silicates precipitated in sediment-free, Si-undersaturated conditions are highly similar to those observed on ANME-SRB consortia extracted from environmental samples. These observations indicate bona fide silicate precipitation mediated by ANME-SRB consortia and suggest that authigenic silicates may play an important role in the taphonomy of methane seep ecosystems in the rock record.

REFERENCES

Aloisi, G., Pierre, C., Rouchy, J.-M., Foucher, J.-P., and Woodside, J. (2000). Methane-related authigenic carbonates of eastern Mediterranean Sea mud volcanoes and their possible relation to gas hydrate destabilisation. Earth Planet. Sci. Lett. 184, 321–338. doi:10.1016/S0012-821X(00)00322-8.

Barghoorn, E. S., and Tyler, S. A. (1965). Microorganisms from the Gunflint Chert. Science 147, 563–575. doi:10.1126/science.147.3658.563.

Beal, E. J., House, C. H., and Orphan, V. J. (2009). Manganese- and Iron-Dependent Marine Methane Oxidation. Science 325, 184–187. doi:10.1126/science.1169984.

Belton, D. J., Patwardhan, S. V., Annenkov, V. V., Danilovtseva, E. N., and Perry, C. C. (2008). From biosilicification to tailored materials: Optimizing hydrophobic domains and resistance to protonation of polyamines. Proc. Natl. Acad. Sci. 105, 5963–5968. doi:10.1073/pnas.0710809105.

Boetius, A., Ravenschlag, K., Schubert, C. J., Rickert, D., Widdel, F., Gieseke, A., et al. (2000). A marine microbial consortium apparently mediating anaerobic oxidation of methane. Nature 407, 623. doi:10.1038/35036572.

Braissant, O., Decho, A. W., Dupraz, C., Glunk, C., Przekop, K. M., and Visscher, P. T. (2007). Exopolymeric substances of sulfate-reducing bacteria: Interactions with calcium at alkaline pH and implication for formation of carbonate minerals. Geobiology 5, 401–411. doi:10.1111/j.1472-4669.2007.00117.x.

Cai, C., Leu, A. O., Xie, G.-J., Guo, J., Feng, Y., Zhao, J.-X., et al. (2018). A methanotrophic archaeon couples anaerobic oxidation of methane to Fe(III) reduction. ISME J. 12, 1929–1939. doi:10.1038/s41396-018-0109-x.

Callow, R. H. T., and Brasier, M. D. (2009). Remarkable preservation of microbial mats in Neoproterozoic siliciclastic settings: Implications for Ediacaran taphonomic models. Earth-Sci. Rev. 96, 207–219. doi:10.1016/j.earscirev.2009.07.002.

Case, D. H., Pasulka, A. L., Marlow, J. J., Grupe, B. M., Levin, L. A., and Orphan, V. J. (2015). Methane Seep Carbonates Host Distinct, Diverse, and Dynamic Microbial Assemblages. mBio 6. doi:10.1128/mBio.01348-15.

Chen, Y., Li, Y.-L., Zhou, G.-T., Li, H., Lin, Y.-T., Xiao, X., et al. (2014). Biomineralization mediated by anaerobic methane-consuming cell consortia. Sci. Rep. 4, 1–9. doi:10.1038/srep05696.

Cline, J. D. (1969). Spectrophotometric Determination of Hydrogen Sulfide in Natural Waters1. Limnol. Oceanogr. 14, 454–458. doi:10.4319/lo.1969.14.3.0454.

Cock, P. J. A., Antao, T., Chang, J. T., Chapman, B. A., Cox, C. J., Dalke, A., et al. (2009). Biopython: freely available Python tools for computational molecular biology and bioinformatics. Bioinformatics 25, 1422–1423. doi:10.1093/bioinformatics/btp163.

Decho, A. W. (2010). Overview of biopolymer-induced mineralization: What goes on in biofilms? Ecol. Eng. 36, 137–144. doi:10.1016/j.ecoleng.2009.01.003.

Dekas, A. E. (2013). Diazotrophy in the deep: an analysis of the distribution, magnitude, geochemical controls, and biological mediators of deep-sea benthic nitrogen fixation. Div. Geol. Planet. Sci. Ph.D.

Dekas, A. E., Poretsky, R. S., and Orphan, V. J. (2009). Deep-Sea Archaea Fix and Share Nitrogen in Methane-Consuming Microbial Consortia. Science 326, 422–426. doi:10.1126/science.1178223.

Dixit, S., Van Cappellen, P., and van Bennekom, A. J. (2001). Processes controlling solubility of biogenic silica and pore water build-up of silicic acid in marine sediments. Mar. Chem. 73, 333–352. doi:10.1016/S0304-4203(00)00118-3.

Dong, H., Kostka, J. E., and Kim, J. (2003). Microscopic evidence for microbial dissolution of smectite. Clays Clay Miner. 51, 502–512.

Drever, J. I. (1988). The Geochemistry of Natural Waters. 3rd ed. Upper Saddle River, New Jersey: Prentice Hall.

Ettwig, K. F., Zhu, B., Speth, D., Keltjens, J. T., Jetten, M. S. M., and Kartal, B. (2016). Archaea catalyze iron-dependent anaerobic oxidation of methane. Proc. Natl. Acad. Sci. 113, 12792–12796. doi:10.1073/pnas.1609534113.

Fein, J. B., Scott, S., and Rivera, N. (2002). The effect of Fe on Si adsorption by *Bacillus subtilis* cell walls: insights into non-metabolic bacterial precipitation of silicate minerals. Chem. Geol. 182, 265–273. doi:10.1016/S0009-2541(01)00294-7.

Ferris, F. G., Fyfe, W. S., and Beveridge, T. J. (1987). Bacteria as nucleation sites for authigenic minerals in a metal-contaminated lake sediment. Chem. Geol. 63, 225–232. doi:10.1016/0009-2541(87)90165-3.

Furukawa, Y., and O'Reilly, S. E. (2007). Rapid precipitation of amorphous silica in experimental systems with nontronite (NAu-1) and *Shewanella oneidensis* MR-1. Geochim. Cosmochim. Acta 71, 363–377. doi:10.1016/j.gca.2006.09.006.

G.E. Healthcare Life Sciences (2018). Cell Separation Media: Methodology and applications. Uppsala, Sweden: GE Healthcare Bio-Sciences AB.

Girguis, P. R., Cozen, A. E., and DeLong, E. F. (2005). Growth and population dynamics of anaerobic methane-oxidizing archaea and sulfate-reducing bacteria in a continuous-flow bioreactor. Appl. Environ. Microbiol. 71, 3725–3733. doi:10.1128/aem.71.7.3725-3733.2005.

Glasauer, S., Langley, S., and Beveridge, T. J. (2001). Sorption of Fe (Hydr)Oxides to the Surface of *Shewanella putrefaciens*: Cell-Bound Fine-Grained Minerals Are Not Always Formed De Novo. Appl. Environ. Microbiol. 67, 5544–5550. doi:10.1128/aem.67.12.5544-5550.2001.

Gunnarsson, I., and Arnórsson, S. (2000). Amorphous silica solubility and the thermodynamic properties of H4SiO°4 in the range of 0° to 350°C at Psat. Geochim. Cosmochim. Acta 64, 2295–2307. doi:10.1016/S0016-7037(99)00426-3.

Hamana, K., Niitsu, M., Samejima, K., and Matsuzaki, S. (1991). Polyamine Distributions in Thermophilic Eubacteria Belonging to Thermus and Acidothermus. J. Biochem. (Tokyo) 109, 444–449.

Hikida, Y., Suzuki, S., Togo, Y., and Ijiri, A. (2003). An exceptionally well-preserved fossil seep community from the Cretaceous Yezo Group in the Nakagawa area, Hokkaido, northern Japan. Paleontol. Res. 7, 329–342. doi:10.2517/prpsj.7.329.

Himmler, T., Freiwald, A., Stollhofen, H., and Peckmann, J. (2008). Late Carboniferous hydrocarbon-seep carbonates from the glaciomarine Dwyka Group, southern Namibia. Palaeogeogr. Palaeoclimatol. Palaeoecol. 257, 185–197. doi:10.1016/j.palaeo.2007.09.018.

Hugo, R. C., Cady, S. L., and Smythe, W. (2011). The Role of Extracellular Polymeric Substances in the Silicification of Calothrix: Evidence from Microbial Mat Communities in Hot Springs at Yellowstone National Park, USA. Geomicrobiol. J. 28, 667–675. doi:10.1080/01490451.2010.511983.

Iler, R. K. (1979). The Chemistry of Silica: Solubility, Polymerization, Colloid and Surface Properties, and Biochemistry. New York: Wiley.

Kaim, A., Jenkins, R. G., and WarÉN, A. (2008). Provannid and provannid-like gastropods from the Late Cretaceous cold seeps of Hokkaido (Japan) and the fossil record of the Provannidae (Gastropoda: Abyssochrysoidea). Zool. J. Linn. Soc. 154, 421–436. doi:10.1111/j.1096-3642.2008.00431.x.

Knittel, K., and Boetius, A. (2009). Anaerobic Oxidation of Methane: Progress with an Unknown Process. Annu. Rev. Microbiol. 63, 311–334. doi:10.1146/annurev.micro.61.080706.093130.

Knott, J. M. (2009). Biosynthesis of long-chain polyamines by crenarchaeal polyamine synthases from Hyperthermus butylicus and Pyrobaculum aerophilum. FEBS Lett 583, 3519–24. doi:10.1016/j.febslet.2009.10.014.

Köhler, B., Singer, A., and Stoffers, P. (1994). Biogenic nontronite from marine white smoker chimneys. Clays Clay Miner. 42, 689–701.

Köhler, S., Irmer, G., Kleeberg, R., Monecke, J., Herzig, P. M., and Schulz, B. (1999). Melanophlogite from the Cascadia accretionary prism, offshore Oregon: First occurrence in a cold seep environment. Berichte Dtsch. Mineral. Ges. 11, 129.

Konhauser, K. O., Fyfe, W. S., Ferris, F. G., and Beveridge, T. J. (1993). Metal sorption and mineral precipitation by bacteria in two Amazonian river systems: Rio Solimões and Rio Negro, Brazil. Geology 21, 1103–1106. doi:10.1130/0091-7613(1993)021<1103:MSAMPB>2.3.CO;2.

Konhauser, K. O., Schultze-Lam, S., Ferris, F. G., Fyfe, W. S., Longstaffe, F. J., and Beveridge, T. J. (1994). Mineral precipitation by epilithic biofilms in the speed river, ontario, Canada. Appl Env. Microbiol 60, 549–53.

Konhauser, K. O., and Urrutia, M. M. (1999). Bacterial clay authigenesis: a common biogeochemical process. Chem. Geol. 161, 399–413. doi:10.1016/S0009-2541(99)00118-7.

Krause, S., Liebetrau, V., Gorb, S., Sánchez-Román, M., McKenzie, J. A., and Treude, T. (2012). Microbial nucleation of Mg-rich dolomite in exopolymeric substances under anoxic modern seawater salinity: New insight into an old enigma. Geology 40, 587–590. doi:10.1130/G32923.1.

Kröger, N., Deutzmann, R., Bergsdorf, C., and Sumper, M. (2000). Species-specific polyamines from diatoms control silica morphology. Proc. Natl. Acad. Sci. 97, 14133–14138. doi:10.1073/pnas.260496497.

Kroger, N., Deutzmann, R., and Sumper, M. (2001). Silica-precipitating peptides from diatoms. The chemical structure of silaffin-A from Cylindrotheca fusiformis. J Biol Chem 276, 26066–70. doi:10.1074/jbc.M102093200.

Kuechler, R. R., Birgel, D., Kiel, S., Freiwald, A., Goedert, J. L., Thiel, V., et al. (2012). Miocene methane-derived carbonates from southwestern Washington, USA and a model for silicification at seeps. Lethaia 45, 259–273. doi:10.1111/j.1502-3931.2011.00280.x.

Lalonde, S. V., Konhauser, K. O., Reysenbach, A.-L., and Ferris, F. G. (2005). The experimental silicification of Aquificales and their role in hot spring sinter formation. Geobiology 3, 41–52. doi:10.1111/j.1472-4669.2005.00042.x.

Lazzeri, K. E., Bebout, G. E., and Geiger, C. A. (2017). Nitrogen and carbon concentrations and isotopic compositions of the silica clathrate melanophlogite. Am. Mineral. 102, 686–689. doi:10.2138/am-2017-5876.

Leu, A. O., Cai, C., McIlroy, S. J., Southam, G., Orphan, V. J., Yuan, Z., et al. (2020). Anaerobic methane oxidation coupled to manganese reduction by members of the Methanoperedenaceae. ISME J. 14, 1030–1041. doi:10.1038/s41396-020-0590-x.

Li, Y.-L., Vali, H., Sears, S. K., Yang, J., Deng, B., and Zhang, C. L. (2004). Iron reduction and alteration of nontronite NAu-2 by a sulfate-reducing bacterium1 1Associate editor: J. B. Fein. Geochim. Cosmochim. Acta 68, 3251–3260. doi:10.1016/j.gca.2004.03.004.

Loyd, S. J., Sample, J., Tripati, R. E., Defliese, W. F., Brooks, K., Hovland, M., et al. (2016). Methane seep carbonates yield clumped isotope signatures out of equilibrium with formation temperatures. Nat. Commun. 7, 12274. doi:10.1038/ncomms12274.

Luff, R., and Wallmann, K. (2003). Fluid flow, methane fluxes, carbonate precipitation and biogeochemical turnover in gas hydrate-bearing sediments at Hydrate Ridge, Cascadia Margin: numerical modeling and mass balances. Geochim. Cosmochim. Acta 67, 3403–3421. doi:10.1016/S0016-7037(03)00127-3.

Marlow, J. J., Steele, J. A., Ziebis, W., Thurber, A. R., Levin, L. A., and Orphan, V. J. (2014). Carbonate-hosted methanotrophy represents an unrecognized methane sink in the deep sea. Nat. Commun. 5, 5094. doi:10.1038/ncomms6094.

Mason, O. U., Case, D. H., Naehr, T. H., Lee, R. W., Thomas, R. B., Bailey, J. V., et al. (2015). Comparison of Archaeal and Bacterial Diversity in Methane Seep Carbonate Nodules and Host Sediments, Eel River Basin and Hydrate Ridge, USA. Microb. Ecol. 70, 766–784. doi:10.1007/s00248-015-0615-6.

McGlynn, S. E., Chadwick, G. L., Kempes, C. P., and Orphan, V. J. (2015). Single cell activity reveals direct electron transfer in methanotrophic consortia. Nature 526, 531–535. doi:10.1038/nature15512.

McGlynn, S. E., Chadwick, G. L., O'Neill, A., Mackey, M., Thor, A., Deerinck, T. J., et al. (2018). Subgroup Characteristics of Marine Methane-Oxidizing ANME-2 Archaea and Their Syntrophic Partners as Revealed by Integrated Multimodal Analytical Microscopy. Appl. Environ. Microbiol. 84, e00399-18. doi:10.1128/AEM.00399-18.

Mera, M. U., and Beveridge, T. J. (1993). Mechanism of silicate binding to the bacterial cell wall in *Bacillus subtilis*. J. Bacteriol. 175, 1936–1945.

Meulepas, R. J. W., Jagersma, C. G., Gieteling, J., Buisman, C. J. N., Stams, A. J. M., and Lens, P. N. L. (2009). Enrichment of anaerobic methanotrophs in sulfate-reducing membrane bioreactors. Biotechnol. Bioeng. 104, 458–470. doi:10.1002/bit.22412.

Michael, A. J. (2011). Molecular machines encoded by bacterially-derived multi-domain gene fusions that potentially synthesize, N-methylate and transfer long chain polyamines in diatoms. FEBS Lett. 585, 2627–2634. doi:10.1016/j.febslet.2011.07.038.

Michaelis, W., Seifert, R., Nauhaus, K., Treude, T., Thiel, V., Blumenberg, M., et al. (2002). Microbial Reefs in the Black Sea Fueled by Anaerobic Oxidation of Methane. Science 297, 1013–1015. doi:10.1126/science.1072502.

Michalopoulos, P., and Aller, R. C. (2004). Early diagenesis of biogenic silica in the Amazon delta: alteration, authigenic clay formation, and storage. Geochim. Cosmochim. Acta 68, 1061–1085. doi:10.1016/j.gca.2003.07.018.

Minguet, E. G., Vera-Sirera, F., Marina, A., Carbonell, J., and Blázquez, M. A. (2008). Evolutionary Diversification in Polyamine Biosynthesis. Mol. Biol. Evol. 25, 2119–2128. doi:10.1093/molbev/msn161.

Miyajima, Y., Watanabe, Y., Yanagisawa, Y., Amano, K., Hasegawa, T., and Shimobayashi, N. (2016). A late Miocene methane-seep deposit bearing methane-trapping silica minerals at Joetsu, central Japan. Palaeogeogr. Palaeoclimatol. Palaeoecol. 455, 1–15. doi:10.1016/j.palaeo.2016.05.002.

Moore, D. M., and Reynolds, R. C. (1997). X-Ray Diffraction and the Identification and Analysis of Clay Minerals. New York: Oxford University Press.

Motomura, K., Ikeda, T., Matsuyama, S., Abdelhamid, M. A. A., Tanaka, T., Ishida, T., et al. (2016). The C-Terminal Zwitterionic Sequence of CotB1 Is Essential for Biosilicification of the *Bacillus cereus* Spore Coat. J. Bacteriol. 198, 276–282. doi:10.1128/jb.00447-15.

Naehr, T. H., Eichhubl, P., Orphan, V. J., Hovland, M., Paull, C. K., Ussler, W., et al. (2007). Authigenic carbonate formation at hydrocarbon seeps in continental margin sediments: A comparative study. Deep Sea Res. Part II Top. Stud. Oceanogr. 54, 1268–1291. doi:10.1016/j.dsr2.2007.04.010.

Nauhaus, K., Albrecht, M., Elvert, M., Boetius, A., and Widdel, F. (2007). In vitro cell growth of marine archaeal-bacterial consortia during anaerobic oxidation of methane with sulfate. Environ. Microbiol. 9, 187–196. doi:10.1111/j.1462-2920.2006.01127.x.

Newman, S. A., Mariotti, G., Pruss, S., and Bosak, T. (2016). Insights into cyanobacterial fossilization in Ediacaran siliciclastic environments. Geology 44, 579–582. doi:10.1130/G37791.1.

Ohnuma, M., Ganbe, T., Terui, Y., Niitsu, M., Sato, T., Tanaka, N., et al. (2011). Crystal structures and enzymatic properties of a triamine/agmatine aminopropyltransferase from Thermus thermophilus. J Mol Biol 408, 971–86. doi:10.1016/j.jmb.2011.03.025.

O'Reilly, S. E., Watkins, J., and Furukawa, Y. (2005). Secondary mineral formation associated with respiration of nontronite, NAu-1 by iron reducing bacteria. Geochem. Trans. 6, 67–67. doi:10.1186/1467-4866-6-67.

Orphan, V. J., Hinrichs, K.-U., Ussler, W., Paull, C. K., Taylor, L. T., Sylva, S. P., et al. (2001a). Comparative Analysis of Methane-Oxidizing Archaea and Sulfate-Reducing Bacteria in Anoxic Marine Sediments. Appl. Environ. Microbiol. 67, 1922–1934. doi:10.1128/AEM.67.4.1922-1934.2001.

Orphan, V. J., House, C. H., Hinrichs, K.-U., McKeegan, K. D., and DeLong, E. F. (2001b). Methane-Consuming Archaea Revealed by Directly Coupled Isotopic and Phylogenetic Analysis. Science 293, 484–487. doi:10.1126/science.1061338.

Orphan, V. J., House, C. H., Hinrichs, K.-U., McKeegan, K. D., and DeLong, E. F. (2002). Multiple archaeal groups mediate methane oxidation in anoxic cold seep sediments. Proc. Natl. Acad. Sci. 99, 7663–7668. doi:10.1073/pnas.072210299.

Orphan, V. J., Turk, K. A., Green, A. M., and House, C. H. (2009). Patterns of 15N assimilation and growth of methanotrophic ANME-2 archaea and sulfate-reducing bacteria within structured syntrophic consortia revealed by FISH-SIMS. Environ. Microbiol. 11, 1777–1791. doi:10.1111/j.1462-2920.2009.01903.x.

Peckmann, J., Goedert, J. L., Thiel, V., Michaelis, W., and Reitner, J. (2002). A comprehensive approach to the study of methane-seep deposits from the Lincoln Creek Formation, western Washington State, USA. Sedimentology 49, 855–873. doi:10.1046/j.1365-3091.2002.00474.x.

Pernthaler, A., Dekas, A. E., Brown, C. T., Goffredi, S. K., Embaye, T., and Orphan, V. J. (2008). Diverse syntrophic partnerships from deep-sea methane vents revealed by direct cell capture and metagenomics. Proc. Natl. Acad. Sci. U. S. A. 105, 7052–7057. doi:10.1073/pnas.0711303105.

Pernthaler, J., Glöckner, F.-O., Schönhuber, W., and Amann, R. (2001). "Fluorescence in situ hybridization (FISH) with rRNA-targeted oligonucleotide probes," in Methods in Microbiology Marine Microbiology. (Academic Press), 207–226. doi:10.1016/S0580-9517(01)30046-6.

Phoenix, V. R., Konhauser, K. O., and Ferris, F. G. (2003). Experimental study of iron and silica immobilization by bacteria in mixed Fe-Si systems: implications for microbial silicification in hot springs. Can. J. Earth Sci. 40, 1669–1678. doi:10.1139/e03-044.

Phoenix, V. R., Martinez, R. E., Konhauser, K. O., and Ferris, F. G. (2002). Characterization and Implications of the Cell Surface Reactivity of Calothrix sp. Strain KC97. Appl. Environ. Microbiol. 68, 4827–4834. doi:10.1128/aem.68.10.4827-4834.2002.

Reeburgh, W. S. (2007). Oceanic Methane Biogeochemistry. Chem. Rev. 107, 486–513. doi:10.1021/cr050362v.

Richthammer, P., Börmel, M., Brunner, E., and van Pée, K.-H. (2011). Biomineralization in Diatoms: The Role of Silacidins. ChemBioChem 12, 1362–1366. doi:10.1002/cbic.201000775.

Scheffel, A., Poulsen, N., Shian, S., and Kröger, N. (2011). Nanopatterned protein microrings from a diatom that direct silica morphogenesis. Proc. Natl. Acad. Sci. 108, 3175–3180. doi:10.1073/pnas.1012842108.

Scheller, S., Yu, H., Chadwick, G. L., McGlynn, S. E., and Orphan, V. J. (2016). Artificial electron acceptors decouple archaeal methane oxidation from sulfate reduction. Science 351, 703–707. doi:10.1126/science.aad7154.

Schink, B. (1997). Energetics of syntrophic cooperation in methanogenic degradation. Microbiol. Mol. Biol. Rev. 61, 262–280.

Schreiber, L., Holler, T., Knittel, K., Meyerdierks, A., and Amann, R. (2010). Identification of the dominant sulfate-reducing bacterial partner of anaerobic methanotrophs of the ANME-2 clade. Environ. Microbiol. 12, 2327–2340. doi:10.1111/j.1462-2920.2010.02275.x.

Siever, R., and Woodford, N. (1973). Sorption of silica by clay minerals. Geochim. Cosmochim. Acta 37, 1851–1880. doi:10.1016/0016-7037(73)90146-4.

Sivan, O., Antler, G., Turchyn, A. V., Marlow, J. J., and Orphan, V. J. (2014). Iron oxides stimulate sulfate-driven anaerobic methane oxidation in seeps. Proc. Natl. Acad. Sci. 111, E4139–E4147. doi:10.1073/pnas.1412269111.

Skennerton, C. T., Chourey, K., Iyer, R., Hettich, R. L., Tyson, G. W., and Orphan, V. J. (2017). Methane-Fueled Syntrophy through Extracellular Electron Transfer: Uncovering the Genomic Traits Conserved within Diverse Bacterial Partners of Anaerobic Methanotrophic Archaea. mBio 8, e00530-17. doi:10.1128/mBio.00530-17.

Smrzka, D., Kraemer, S. M., Zwicker, J., Birgel, D., Fischer, D., Kasten, S., et al. (2015). Constraining silica diagenesis in methane-seep deposits. Palaeogeogr. Palaeoclimatol. Palaeoecol. 420, 13–26. doi:10.1016/j.palaeo.2014.12.007.

Stahl, D. A., and Amann, R. (1991). "Development and Application of Nucleic Acid Probes in Bacterial Systematics," in Nucleic Acid Techniques in Bacterial Systematics, eds. E. Stackebrandt and M. Goodfellow (Chichester, U.K.: John Wiley & Sons Ltd.), 205–248.

Teichert, B. M. A., Bohrmann, G., and Suess, E. (2005). Chemoherms on Hydrate Ridge — Unique microbially-mediated carbonate build-ups growing into the water column. Palaeogeogr. Palaeoclimatol. Palaeoecol. 227, 67–85. doi:10.1016/j.palaeo.2005.04.029.

Thiagarajan, N., Crémière, A., Blättler, C., Lepland, A., Kirsimäe, K., Higgins, J., et al. (2020). Stable and Clumped Isotope Characterization of Authigenic Carbonates in Methane Cold Seep Environments. Geochim. Cosmochim. Acta. doi:10.1016/j.gca.2020.03.015.

Tréguer, P. J., and De La Rocha, C. L. (2013). The World Ocean Silica Cycle. Annu. Rev. Mar. Sci. 5, 477–501. doi:10.1146/annurev-marine-121211-172346.

Treude, T., Krüger, M., Boetius, A., and Jørgensen, B. B. (2005). Environmental control on anaerobic oxidation of methane in the gassy sediments of Eckernförde Bay (German Baltic). Limnol. Oceanogr. 50, 1771–1786. doi:10.4319/lo.2005.50.6.1771.

Treude, T., Orphan, V., Knittel, K., Gieseke, A., House, C. H., and Boetius, A. (2007). Consumption of Methane and CO2 by Methanotrophic Microbial Mats from Gas Seeps of the Anoxic Black Sea. Appl. Environ. Microbiol. 73, 2271–2283. doi:10.1128/AEM.02685-06.

Urrutia, M. M., and Beveridge, T. J. (1994). Formation of fine-grained metal and silicate precipitates on a bacterial surface (*Bacillus subtilis*). Chem. Geol. 116, 261–280. doi:10.1016/0009-2541(94)90018-3.

Van Cappellen, P., and Qiu, L. (1997). Biogenic silica dissolution in sediments of the Southern Ocean. I. Solubility. Deep Sea Res. Part II Top. Stud. Oceanogr. 44, 1109–1128. doi:10.1016/S0967-0645(96)00113-0.

Visscher, P. T., Reid, R. P., and Bebout, B. M. (2000). Microscale observations of sulfate reduction: Correlation of microbial activity with lithified micritic laminae in modern marine stromatolites. Geology 28, 919–922. doi:10.1130/0091-7613(2000)28<919:MOOSRC>2.0.CO;2.

Wegener, G., Krukenberg, V., Riedel, D., Tegetmeyer, H. E., and Boetius, A. (2015). Intercellular wiring enables electron transfer between methanotrophic archaea and bacteria. Nature 526, 587–590. doi:10.1038/nature15733.

Wenzl, S., Hett, R., Richthammer, P., and Sumper, M. (2008). Silacidins: Highly Acidic Phosphopeptides from Diatom Shells Assist in Silica Precipitation In Vitro. Angew. Chem. Int. Ed. 47, 1729–1732. doi:10.1002/anie.200704994.

Yee, N., Phoenix, V. R., Konhauser, K. O., Benning, L. G., and Ferris, F. G. (2003). The effect of cyanobacteria on silica precipitation at neutral pH: implications for bacterial silicification in geothermal hot springs. Chem. Geol. 199, 83–90. doi:10.1016/S0009-2541(03)00120-7.

Yu, N. Y., Wagner, J. R., Laird, M. R., Melli, G., Rey, S., Lo, R., et al. (2010). PSORTb 3.0: improved protein subcellular localization prediction with refined localization subcategories and predictive capabilities for all prokaryotes. Bioinformatics 26, 1608–15. doi:10.1093/bioinformatics/btq249.

Zabel, M., Boetius, A., Emeis, K. C., Ferdelman, T. G., and Spieß, V. (2008). RV METEOR Cruise Report M76/L1, M76/L2, M76/L3a+b, PROSA process Studies in the Eastern South Atlantic. DFG Senatskommission für Ozeanographie.

Zhang, G., Dong, H., Kim, J., and Eberl, D. D. (2007). Microbial reduction of structural Fe3+ in nontronite by a thermophilic bacterium and its role in promoting the smectite to illite reaction. Am. Mineral. 92, 1411–1419. doi:10.2138/am.2007.2498.

Zhang, Y., Henriet, J.-P., Bursens, J., and Boon, N. (2010). Stimulation of in vitro anaerobic oxidation of methane rate in a continuous high-pressure bioreactor. Bioresour. Technol. 101, 3132–3138. doi:10.1016/j.biortech.2009.11.103.

Zhang, Y., Maignien, L., Zhao, X., Wang, F., and Boon, N. (2011). Enrichment of a microbial community performing anaerobic oxidation of methane in a continuous high-pressure bioreactor. BMC Microbiol. 11, 137. doi:10.1186/1471-2180-11-137.

SUPPLEMENTAL FIGURES

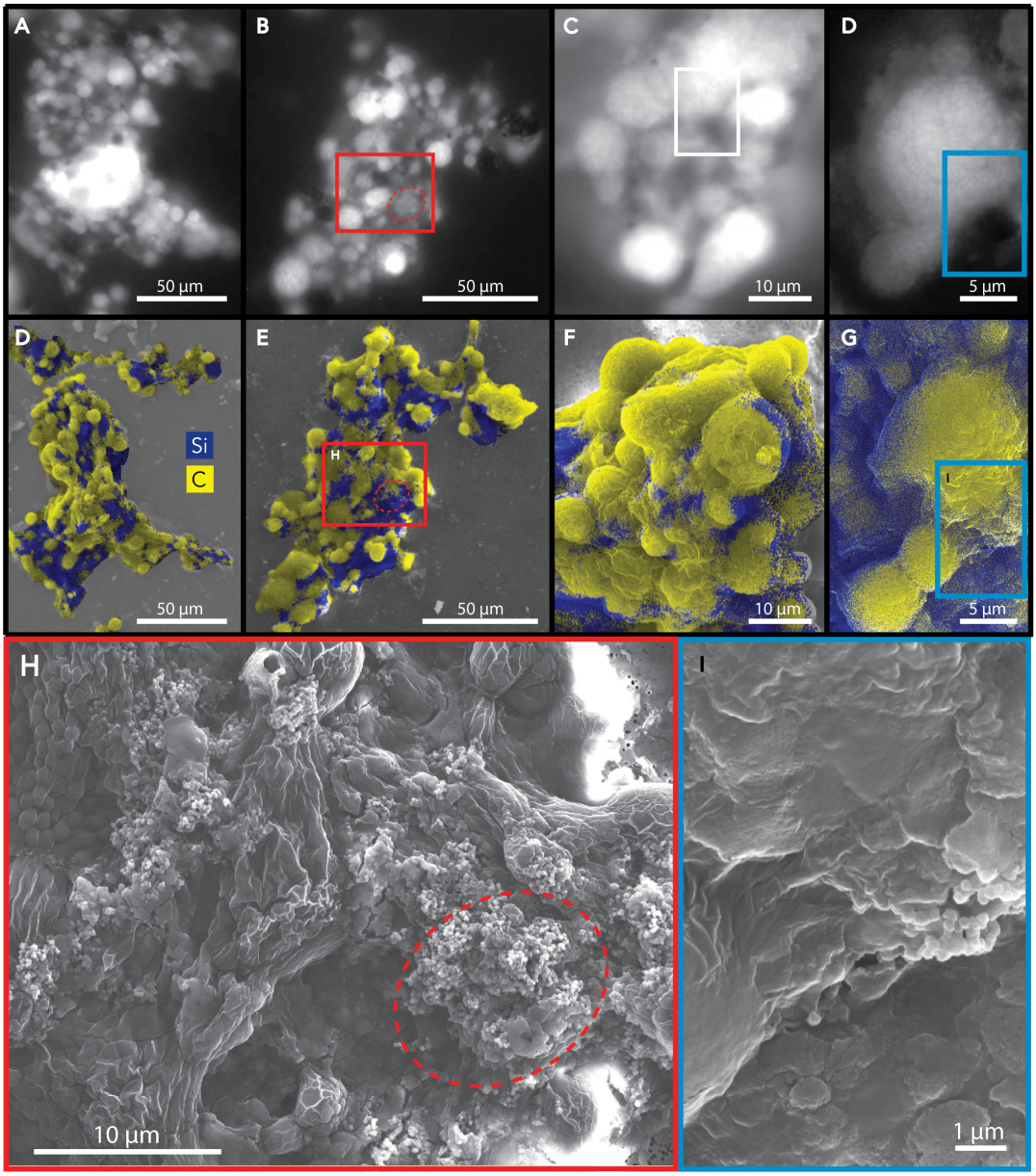

Supplemental Figure 1. Epifluorescence (DAPI-stained) (A-D), SEM-EDS (D-I) imagery documenting spatial distribution of silicates between consortia (consisting of ANME-2a/b and SEEP-SRB1, based on 16S rRNA amplicon sequencing, Fig. S6) grown under sediment-free conditions. SEM-EDS compositional maps demonstrate the common appearance of Si-rich domains between consortia. Detailed SEM imagery (H-I) corroborates other SEM and TEM imagery demonstrating the appearance of consortium-attached silicates as ~200 nm semispherical particles often intergrown and encrusting consortia.

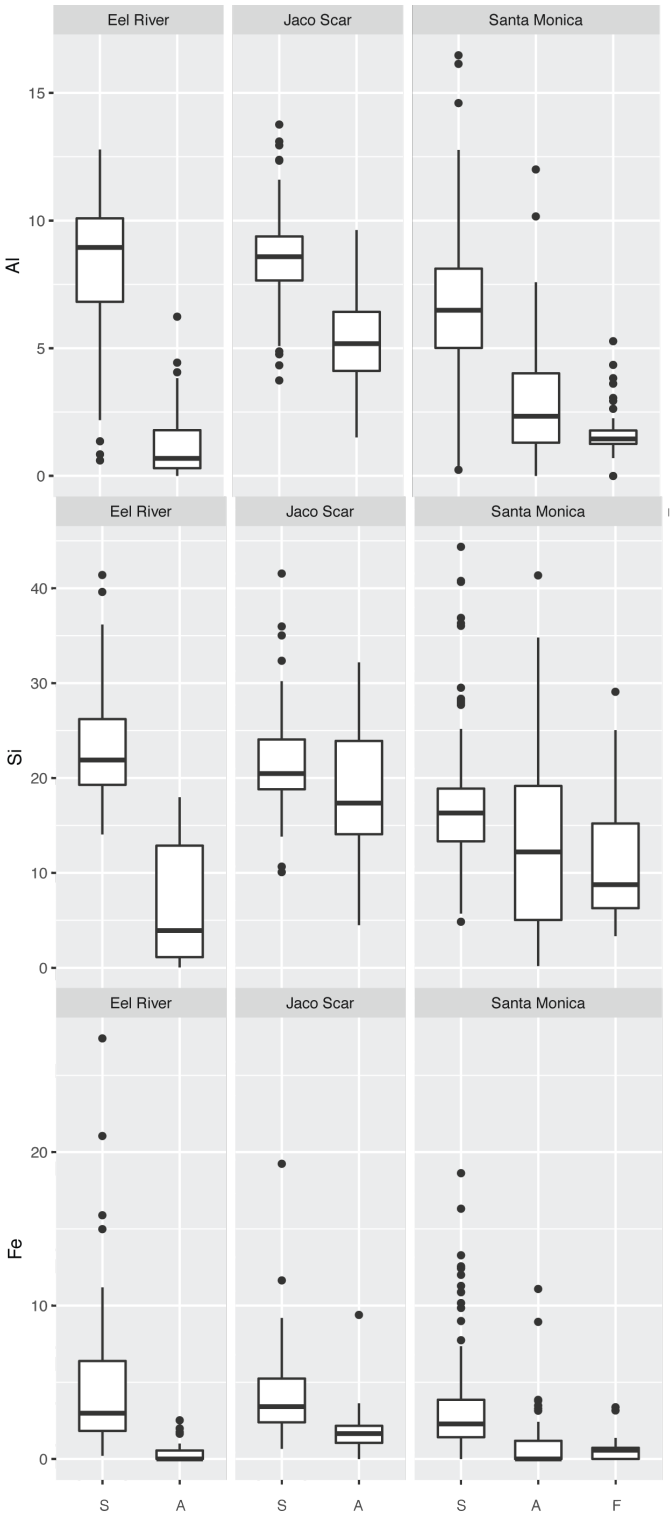

Supplemental Figure 2. EDS compositional data of silicates attached to consortia sourced directly from methane seep sediments (A) or grown under sediment-free conditions (F), demonstrating the Si-rich and Al- and Fe- poor nature of these phases.

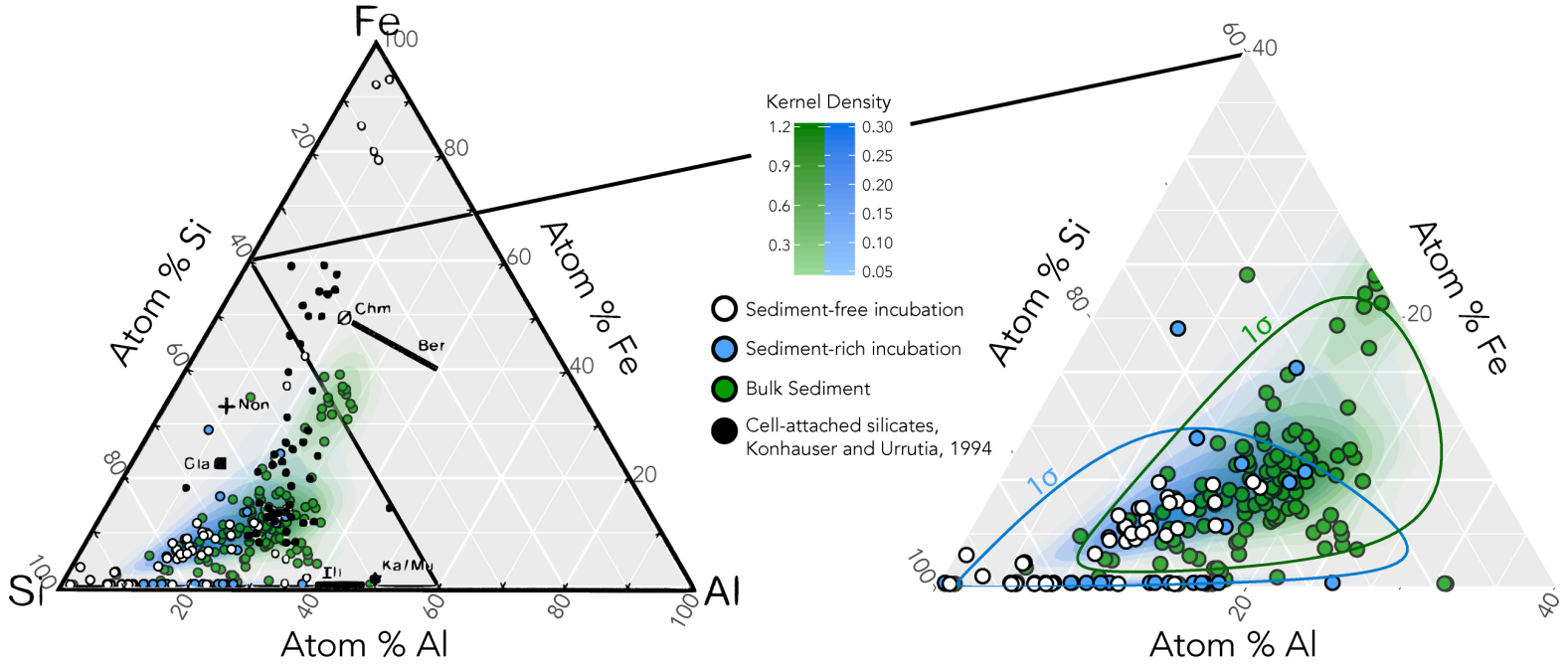

Supplemental Figure 3. EDS compositional data visualized on an Fe-Al-Si ternary plot of silicates attached to consortia sourced from Santa Monica Basin methane seep sediments or sediment-free incubations, demonstrating (left panel) significant compositional differences between these consortium-attached silicates, bulk methane seep sediment, and previously-observed silicates attached to bacterial cell walls (Konhauser and Urrutia, 1999). ANME-SRB consortium-attached silicates are significantly more Si-rich and Fe- and Al- poor than those previously observed attached to bacterial cell exteriors.

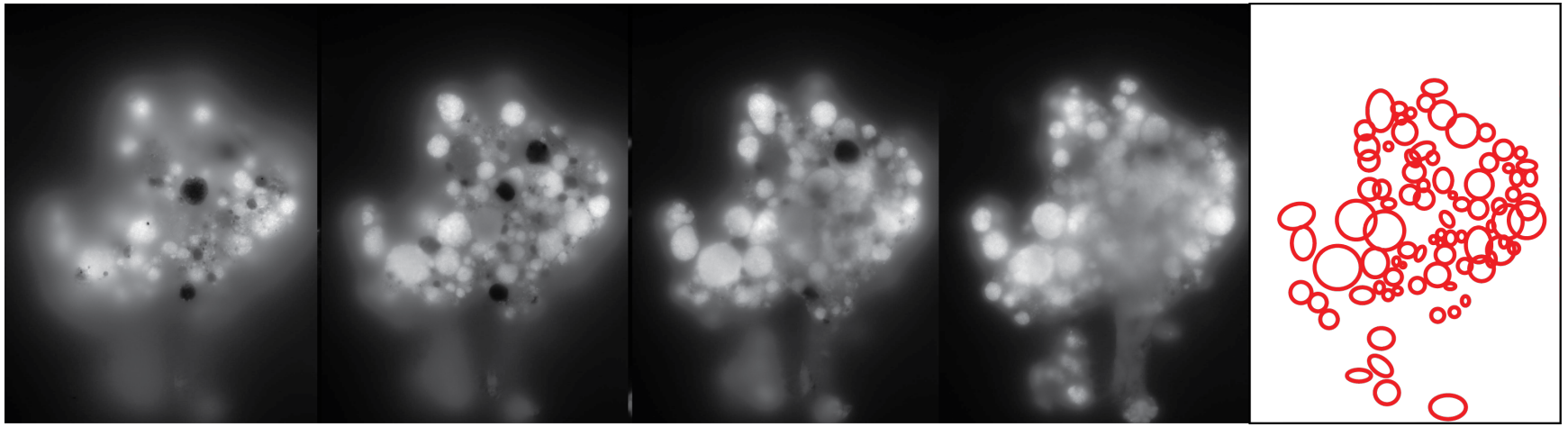

Supplemental Figure 4. Epifluorescence (using DAPI) imagery of a large consortium cluster grown under sediment-free conditions, demonstrating the method by which consortia were counted to use as an input to the growth model (Fig. 6). Consortia were counted by inspection of images taken on different focal planes of the epifluorescence microscope.

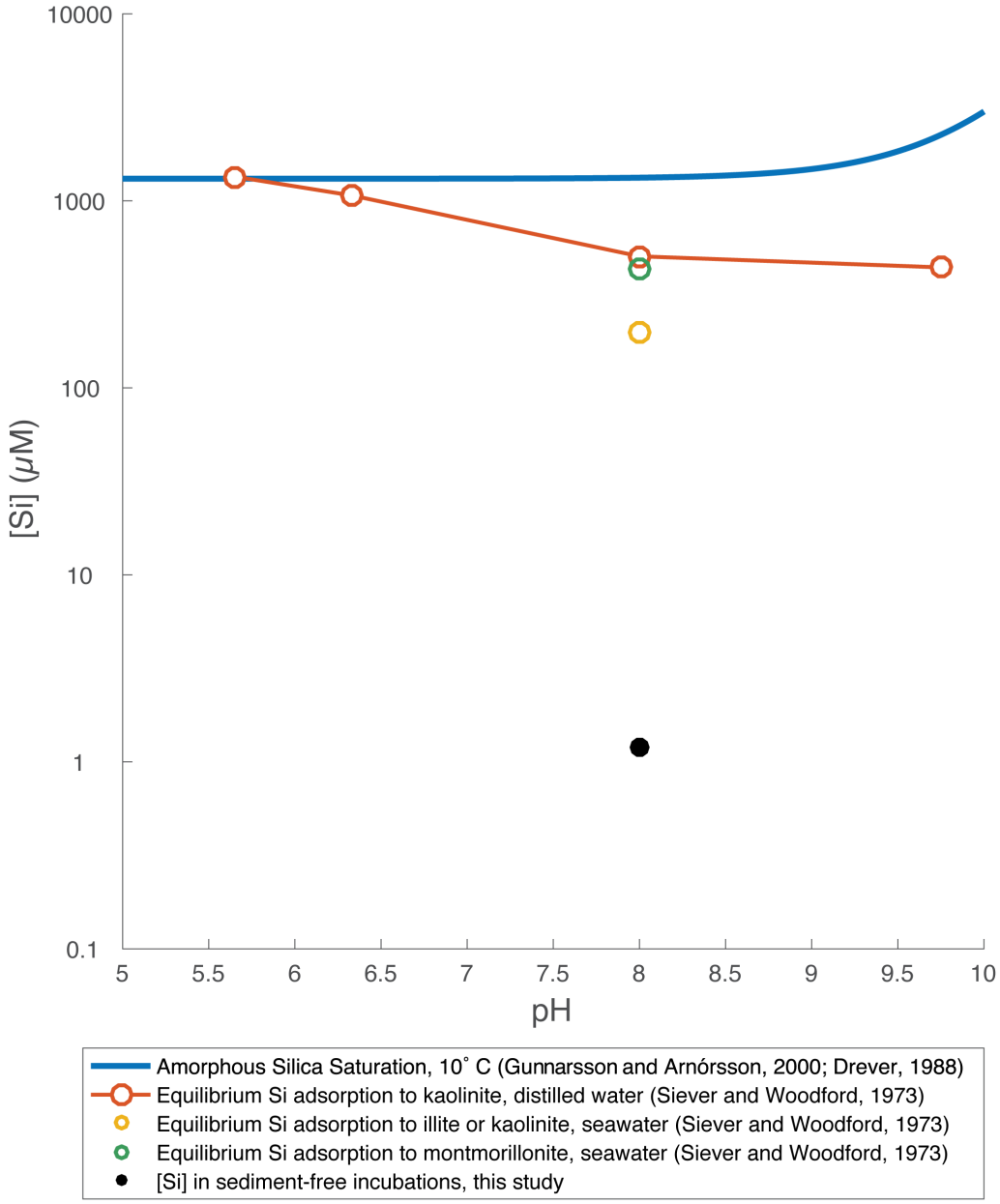

Supplemental Figure 5. Comparison between [Si] measured in media of sediment-free incubations of ANME-SRB consortia examined in this study and theoretical amorphous silica saturation (Drever, 1988; Gunnarsson and Arnórsson, 2000) and equilibrium Si adsorption to aluminosilicate clays (Siever and Woodford, 1973), precluding either abiotic mechanism of Si enrichment of consortium-attached silicates from relevance in the sediment-free incubations examined here.

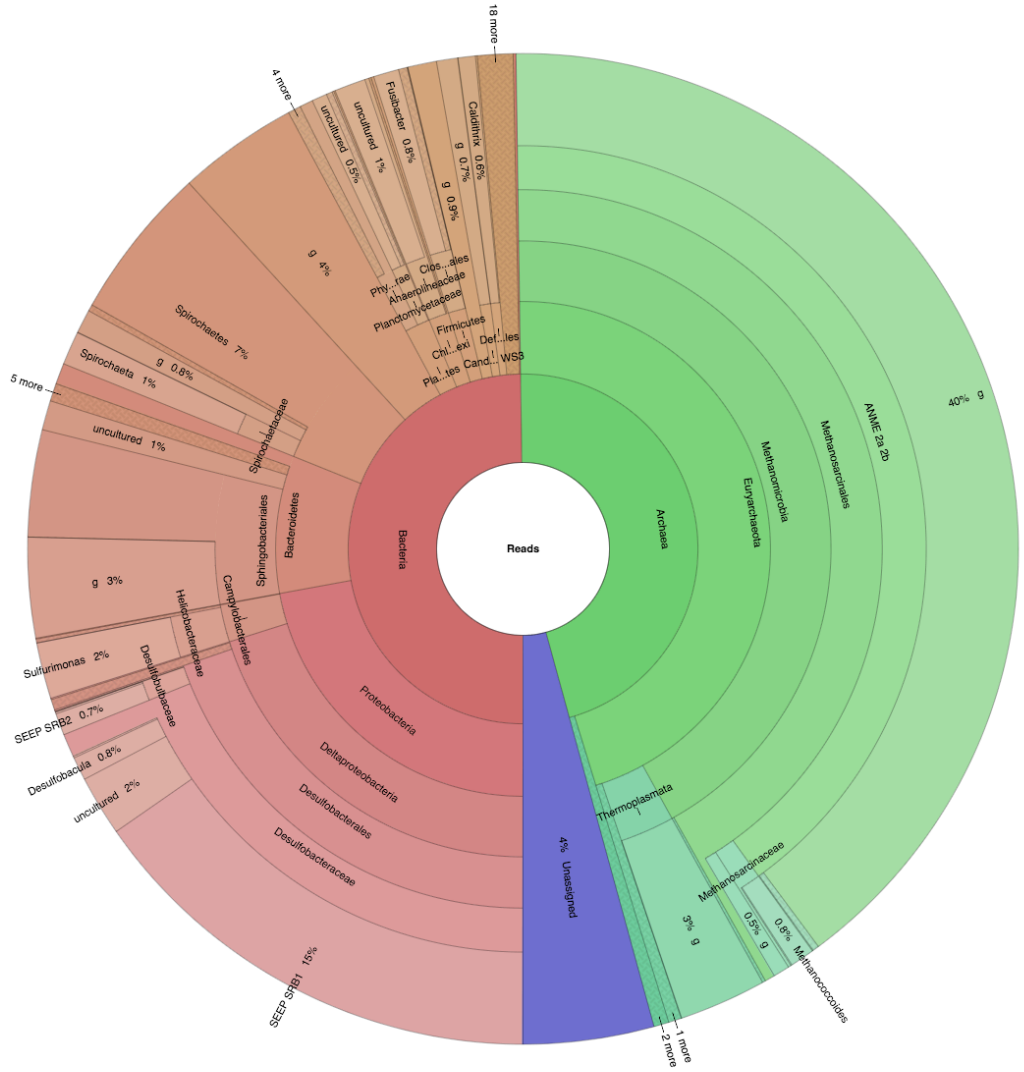

Supplemental Figure 6. Krona chart (Ondov et al., 2011) depicting taxonomic composition of sediment-free incubations based on reads of V4 16S rRNA gene sequences ('iTags'). ANME-2a/b and SEEP SRB1 reads are particularly abundant in this dataset, implying these to be the partner taxa of cell consortia visualized through methods without additional taxonomic resolution (i.e. DAPI stains; Supp. Figs 1,4).

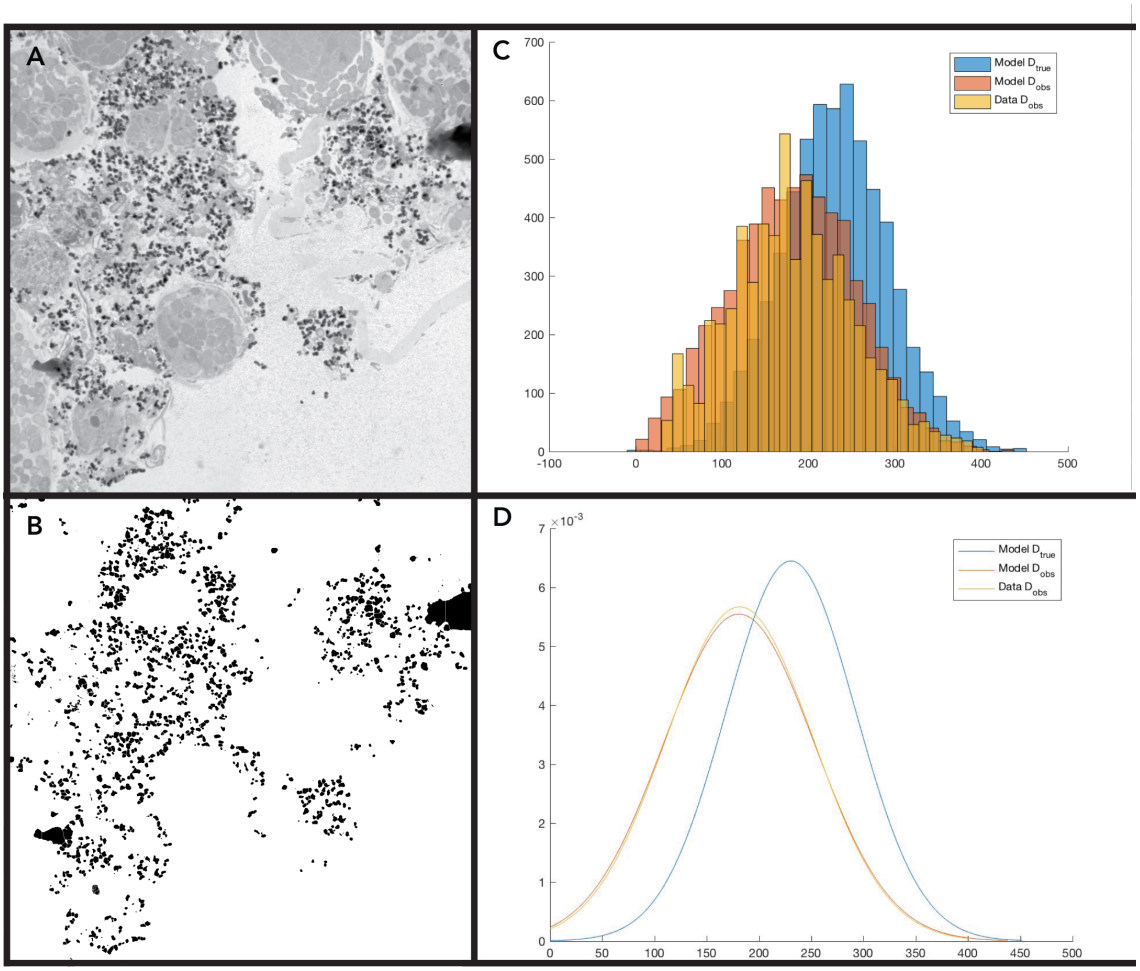

Supplemental Figure 7. TEM imaging of consortium-attached silicates (A) processed in imageJ by thresholding and watershed analysis to obtain raw data (B) for a Markov Chain Monte Carlo (MCMC)-based approach to measure true particle size of subspherical consortium attached silicates. Diameters measured directly from raw TEM data underestimate true particle size, as random cross-sections through spheres with any size distribution are more likely to intersect spheres above or below sphere equators. MCMC estimation of sphere diameter (C-D) is calculated to be (230±62 nm), precluding this phase to be a contaminant such as Percoll (particle size 15-30 nm).